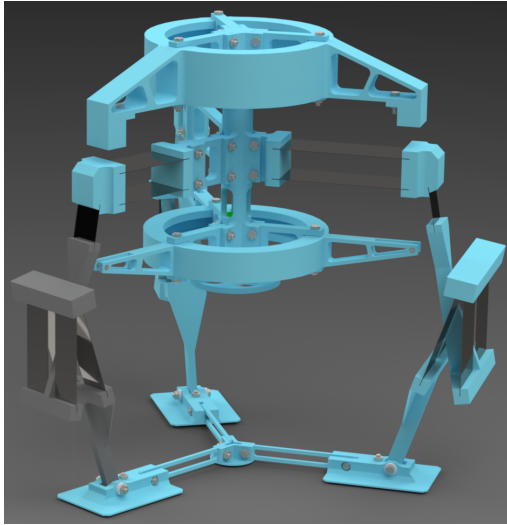


Employing Space Borne Compliant Mechanics: A Compliant Lunar Jumper

Mekelweg 2, Delft 2628 CD, January 20, 2025

Sil Barendregt, Roman Bosch, Fabio Milazzo, Martijn Schrama



Abstract—Lunar exploration vessels traditionally feature wheels to propel themselves forward. This paper proposes a novel kind of Lunar exploration robot that traverses the Lunar terrain by means of jumping. After deriving an optimal kinematic solution, the mechanism was turned into a compliant mechanism. Combining classical mechanics with compliant synthesis yielded an unconventional and innovative leg design. The model was numerically approximated by means of PRBM modeling and verified using FEM and F/D measurement tests. After several design iterations, a final design was derived and its functionality was ascertained. The project yielded a notably robust PRBM model and physical prototype capable of demonstrating the governing mechanics and functionality. Using only one actuator, the robot employs non-linear force-displacement relations to achieve directionality. During the project, careful attention was given to interpreting results and tools like the PRBM were consciously used to investigate and solve discrepancies between models and results.

Index Terms—Jumping Robot, Compliant Mechanics, Kinematic and PRBM Optimization, Non-linear Actuator

INTRODUCTION

Humans have an internal drive to explore our solar system. The number of missions to the Moon is increasing. To acquire significant data during these missions, one needs an efficient vehicle to travel the Lunar landscape, a hard task due to the roughness of the terrain. Traditional rovers use wheels to move over the surface, limiting the area that can be studied. A rover utilizing jumping locomotion would significantly increase this area by its ability to jump over obstacles like valleys or large rocks, giving it the ability to reach places that other rovers would have to avoid. Besides, the jumping locomotion on the Moon would decrease energy consumption as energy losses due to moving over

loose terrain are eliminated. According to Savu (2006), a “Lunar Jumper type vehicle is feasible to be built and to perform Lunar explorations for long duration” [1].

A compliant mechanism uses the flexible elastic regime of materials to transmit input deformation from an actuator to an output deformation [2]. To stress the importance of using a compliant mechanism for this application, a few advantages are stated. First, the Lunar landscape is harsh, with ultra-fine abrasive particles which can damage moving components, while maintenance is out of the question. Compliant mechanisms are more resistant to harsh environments due to the absence of sliding parts. Besides, compliant design offers possibilities for lighter and more compact designs than conventional mechanisms. This results from the fact that the part that hinges also stores energy, eliminating the need for separate mechanisms, greatly reducing mass and thus costs. Furthermore, as compliant mechanisms eliminate sliding components, new manufacturing methods like additive manufacturing may be applied, further decreasing manufacturing complexity and costs. [3].

In this design study, the research objective is to design and build the compliant jumping mechanism of a compliant Lunar jumping robot, which is capable to jump in a desired direction using one single simple rotary actuator. This is done by utilizing nonlinear behavior of the derived compliant mechanism.

The structure of this paper is as follows. In chapter 2, the design process is explained. In chapter 3, performed tests and their results are shown. Finally, in chapter 4 and 5, the discussion and conclusion are shown, respectively.

METHODOLOGY

This chapter describes the method used for designing the compliant mechanism Jumper. First, the functional requirements are determined. Secondly, the morphological chart is created through brainstorm sessions as a team and individual literature research. Following this, the possible solutions are analyzed based on performance criteria. A preliminary concept is then set up, and kinematic analysis is used to determine the dimensions. At this stage, the design remains a rigid body mechanism. Using the Pseudo Rigid Body Model (PRBM) [9] compliant synthesis is performed, allowing for numerical tuning of the final dimensional values for the test design. To verify the design, the Finite Element Model (FEM) software Ansys Mechanical 2024 is used.

Functional Analysis

In this section the functional analysis and corresponding performance metrics of the compliant Jumper are pre-

sented. These metrics are categorized based on product, functional, and design conditional requirements, as detailed in Table I. The main goal of this table is to set measurable design metrics so that, during the development and testing of the design, it can be ascertained whether the Jumper meets its intended requirements. Many of the requirements were quantified using the numerical model from Section PRBM.

- **PROD-XX:** The production metrics define the fundamental performance of the Jumper system to perform as intended.
- **FUNC-XX:** Functional metrics define how the Jumper achieves its functionalities.
- **COND-XX:** Design conditional metrics focus on the conditions that limit the design freedom

TABLE I: Functional analysis

ID	Function	Values
PROD-01	The Jumper traverses a horizontal distance	0.5 m
PROD-02	The Jumper continues to jump in a desired direction after it has been set off with a controlled error	0.1 m
PROD-03	The Jumper traverses a vertical distance	1 m
FUNC-01	The Jumper is reusable	10 cycles
FUNC-02	The Jumper can be “charged” by either itself or an operator	n.a.
FUNC-03	The Jumper can store an amount of mechanical energy	4.91 J
FUNC-04	The Jumper releases the stored energy to jump	60.5 N
FUNC-05	The Jumper protects its equipment from impact	n.a.
FUNC-06	The Jumper is steerable in jumping direction	Differential force
COND-01	Jumper can carry a significant mass	0.5 Kg
COND-02	Jumper stores energy by means of compliant mechanics	n.a.
COND-03	The materials used should be able to endure space conditions	n.a.

Creative Iteration

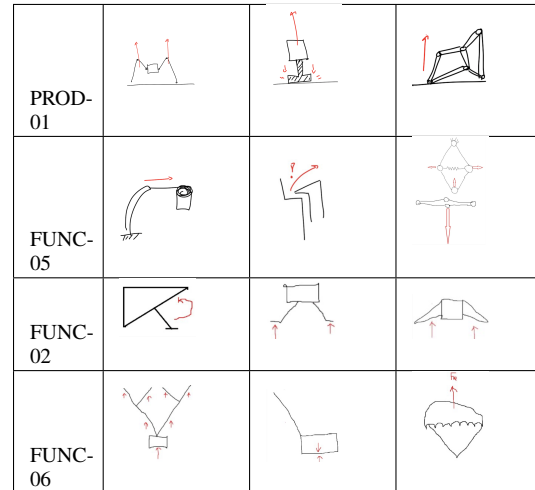
The process of design generation for the compliant Jumper is presented in this chapter. A common approach, the morphological table, is being used to explore various conceptual solutions.

The morphological table serves as a framework to identify potential solutions by breaking down the Jumper's functionality into individual components and filling in the possible design options for each component. The result can be seen in Table II. By combining ideas presented in the table and evaluating them, promising and not always obvious design solutions may be selected that fully satisfy the performance metrics and requirements.

Bio-inspired Design

In millions of years, through constant natural selection, nature has developed her own (compliant) jumping mechanisms. In this subsection the two main jumping patterns are explored. The first can be seen as the ‘pause and leap’ method, as these animals jump and pause afterwards before charging and jumping again [5]. This method can be seen in smaller animals as frogs and insects.

TABLE II: Morphological Chart



Often, bigger animals as kangaroos and bunnies use a different method of locomotion. This method relies on continuous jumping, charging the next jump during landing and thus having no pause in between jumps. Continuous robotic Jumpers have been developed in the past [6], though this method requires a higher level of dynamic control, out of the scope of this paper. Thus, biomechanics for the ‘pause and leap’ method were further explored. A great example is the jumping spider. This small insect specializes in rapid arthropod locomotion to catch prey and flee from danger, [7] and [4]. Simplifying the kinematics of this animal’s legs inspired the Spider concept.

Combined Concepts

Efficiency of locomotion is one of the key advantages of a jumping rover. To achieve this, the force exerted by the output needs to be perpendicular to the surface it wants to jump from, thus eliminating slip in the feet. A path generator can provide a straight, downward direction for the output. This is why in this design study, the mechanism to be derived was of the path-generator kind. Furthermore, simplicity of the actuator mechanism is valued, as it results in a cheaper, more lightweight and reliable system. A single linear or rotary actuator would ideally be sufficient. This objective eventually resulted in multiple simple legs with variable stiffness to steer the robot during the jumping motion.

Choice of Concept

In order to rank the different concepts, a list of criteria was determined. These criteria, combined with their respective weight factor, are listed in table III.

TABLE III: Performance Criteria

ID	Criteria	Goal	Weight
CRIT-01	Reliability	Maximize	9
CRIT-02	Power/Mass ratio	Maximize	8
CRIT-04	Mass	Minimize	6
CRIT-05	Compliance	Maximize	5
CRIT-03	Precision	Maximize	3
CRIT-06	Size	Minimize	3

After weighing the concepts with the performance criteria, two promising concepts were derived: The Spider

and the Triangle.

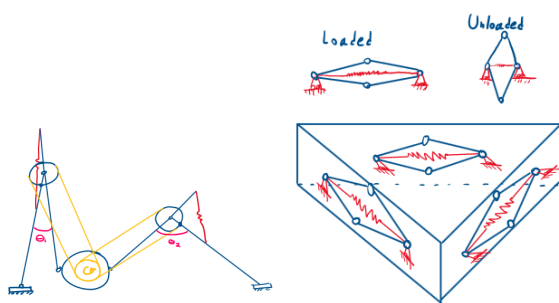


Fig. 1: Concept Spider and Triangle

The Spider and Triangle concept were evaluated using the performance table (Appendix section I-A). Conclusively, the lightweight designed Spider concept scored better on size, mass and power to mass ratio.

Preliminary Concept

As mentioned in the section above, the concept that was deemed the most promising was that of the Spider. One advantage that the Spider had over the other concepts lies in the modular nature of its leg design. The fact that different leg designs can be easily changed, without changing the working principle of the prototype itself, led to a lot of creative freedom for choosing promising leg mechanisms, as can be seen in figure 2.

The jump height of the Spider is mainly governed by the amount of work W that its end effectors do.

$$W = F_s \quad (1)$$

As the work of the jumping motion is determined by the amount of force delivered to the path traveled by some end effector, it can be concluded that the mechanism to derive is of the path-generator category. What this meant for the mechanism synthesis, is that leg-based linkages that maximize end effector travel distance are preferred.

Besides considering end effector path length, the mechanisms also had to take other important requirements into account. The considered requirements that govern these three derived mechanisms are:

- PROD-03: The Jumper traverses a vertical distance
- FUNC-02: The Jumper charges itself (self-straightening)
- FUNC-06: The Jumper can jump in a desired direction (differential leg charging)
- COND-02: The Jumper stores energy by means of compliant mechanics

The three concept were judged on these criteria in a pseudo qualitative way, as listed in table IV.

The end effector path length was estimated by establishing a global member length L and creating preliminary assemblies in SolidWorks. By using a global length for each mechanism, an estimate for the path length that each mechanism would yield could be made.

Taking all four governing criteria into account, mechanism 1 came out on top. The only downside the linkage brought along was the large flex range of the elbow joint. This problem is later addressed in Section "Compliant Synthesis".

Kinematic Analysis

After having settled on mechanism 1 to embody the working mechanics of the Jumper, the kinematics were derived accordingly. Since the Jumper would feature a multiple of the same leg design, only one leg geometry had to be considered. This feat also introduced another important assumption, which is that the center of mass moves purely vertically with respect to the leg's actuation.

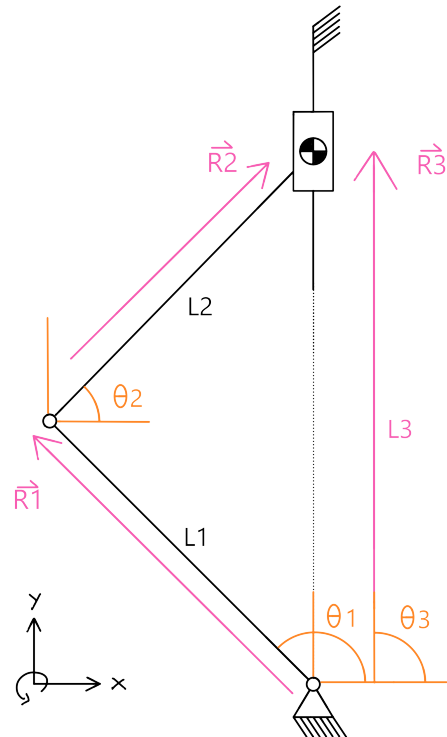


Fig. 3: Kinematics to analyze

The assumptions that govern this model are listed below:

- The center of mass moves purely vertical
- The center of mass stays right above the end effector without any horizontal drift
- There is a no-slip condition between the end effector ("foot") and the ground
- Each leg is geometrically similar to the others

Analyzing the kinematics of a system is done to obtain certain important parameters. These parameters include the system's number of degrees of freedom and kinematic relations. Kinematic relations refer to the relation between member angles and velocity relations. To find the number of degrees of freedom, Gruebler's equation is applied to the system, as shown in equation 2.

$$\#DOF = 3(n - 1) - 2f_1 - f_2 \quad (2)$$

In this equation, n refers to the number of system links and f_1 and f_2 respectively count the number of 1-DOF and 2-DOF joints. The required amount of degrees of freedom is one, which will result in a purely vertical path of the end effector. Applying Gruebler's equation to the system of figure 3 yields the following result:

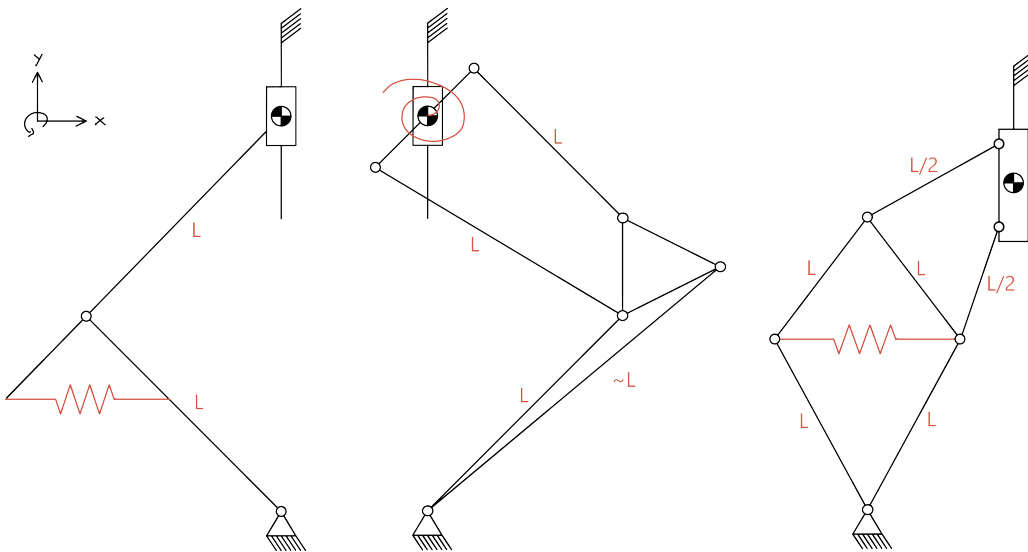


Fig. 2: Mechanisms 1, 2 and 3

Criterion	Mechanism 1	Mechanism 2	Mechanism 3
PROD-03	2 L	1.77 L	0.61 L
FUNC-02	Lowest center mass	Low center mass	High center mass
FUNC-4	Differential force achievable	Differential force achievable	Differential force achievable
COND-02	Large flex range	Continuously rotating part	Small flex range

TABLE IV: Criteria used to judge mechanisms.

$$\#DOF = 3(3 - 1) - 2 * 2 - 1 * 1 = 1 \quad (3)$$

Equation 3 proves that the required amount of degrees of freedom is acquired by the chosen kinematics.

To find the kinematic relations, a vector loop analysis can be applied. Following this method, a 2-dimensional vector is assigned to each linkage member, describing its length and orientation, as shown in equation 4. After establishing these vectors, an end-point of the linkage can be described as a linear combination of the system vectors.

$$\vec{R}_n = |\vec{R}_n| e^{i\angle \vec{R}_n} = L_n e^{i\theta_n} \quad (4)$$

$$\begin{aligned} \Re(\vec{R}_n) &= L_n \cos(\theta_n) \\ \Im(\vec{R}_n) &= L_n \sin(\theta_n) \end{aligned} \quad (5)$$

Applying the vector loop theorem to the system of Figure 3 and choosing the center of mass as the comparison coordinate, results in the following equation:

$$L_1 e^{i\theta_1} + L_2 e^{i\theta_2} = L_3 e^{i\theta_3} \quad (6)$$

Plugging the values into the real and imaginary expansions of equation 12 yields two equations, containing two unknowns, therefore rendering the system solvable (Appendix table X). This system be solved numerically or analytically due to its simplicity to find the kinematic relations.

$$\begin{aligned} L_1 \cos(\theta_1) + L_2 \cos(\theta_2) &= 0 \\ L_1 \sin(\theta_1) + L_2 \sin(\theta_2) &= L_3 \end{aligned} \quad (7)$$

Compliant Synthesis

An important kinematic relation is the relation between the input angle θ_2 and the other system angles. Not only does this yield important information on the system's motion generator aspect behavior, but also does it hint

at the system's potential to be changed into a compliant mechanism.

As compliant mechanics make use of flexing members, the maximum flexure range of a compliant link or joint is limited by geometry and material properties. In order for the material not to fail, the maximum bending stress should remain in the material's elastic region. Following PRBM modeling [9], compliant solutions are limited by:

$$\begin{aligned} \sigma_{max} &= \frac{M E}{I} \\ M &= k_{effective} \theta_{flex} \\ k_{effective} &= (2\gamma K_\Theta) \frac{EI}{l} \end{aligned} \quad (8)$$

Interpreting the results from the kinematic analysis, one can determine the flexure range of joint 2 to be between 0 rad and $\frac{\pi}{2}$ rad with respect to a fabrication angle θ_1 of $\frac{\pi}{2}$ rad Cartesian.

This large flexure range introduces the problem of stiffness versus flexibility. The effective stiffness $k_{effective}$ is both the energy source of the jumping motion as well as the limiting factor for the flexing hinge itself. In order to maximize jumping height, as stated by PROD-01, the amount of energy and thus the effective stiffness should be maximized. Maximizing stiffness however limits the flexure range due to maximum stress relations. Limiting the flexure range results in limited end effector movement and thus less jumping work being done, as described by equation 1. See Appendix item 29 for a better visualization of this problem.

Besides, methods like PRBM can only be linearly used up to about 60 degrees of deflection, further complicifying model simulation.

A solution to this problem was derived from standard

spring mechanics. Considering compliant flexures are essentially similar to regular linear springs, one can reach a desired total effective stiffness of a hinge by tuning several springs in serial and parallel configurations. Classical spring mechanics describe serial and parallel combinations in the following way:

$$\text{Parallel Springs: } k_{eff} = \sum_{n=1}^i k_n \quad (9)$$

$$\text{Serial Springs: } \frac{1}{k_{eff}} = \sum_{n=1}^i \frac{1}{k_n}$$

A rule of thumb is that the effective stiffness can be reduced by linking springs in series and increased by linking them in parallel. Combining these feats can result in a hinge that has the right stiffness and allows for enough motion to increase the jumping work, while respecting the derived kinematics.

After a rigorous design campaign, such a hinge was designed. By taking two sets of serial springs, the right flex range can be reached while maintain proper stiffness. This proof of concept is shown in figure 30. Even though



Fig. 4: Proof of concept model

this new hinge respects the previously derived kinematics to a certain degree, a new kinematics study is required to properly define the motion generator aspect. Applying Gruebler's equation to determine the amount of degrees of freedom resulted in a total amount of 2 degrees of freedom, as demonstrated by equation 10.

$$\#DOF = 3(4 - 1) - 2 * 3 - 1 * 1 = 2 \quad (10)$$

Furthermore, applying the principle of vector analysis to this mechanism can be used to determine the governing system kinematic relations. As the system features 2 degrees of freedom, two input variables have to be selected in order to render the system solvable. The second input was realized by determining the height of the center of mass, described by variable L_4 , to also function as a system input. Realistically, this can be represented by a height detection sensor. The final system parameters are listed in Appendix table IX.

$$\vec{R}_1 + \vec{R}_2 + \vec{R}_3 = \vec{R}_4 \quad (11)$$

$$L_1 e^{i\theta_1} + L_2 e^{i\theta_2} + L_3 e^{i\theta_3} = L_4 e^{i\theta_4} \quad (12)$$

$$\begin{aligned} L_1 \cos(\theta_1) + L_2 \cos(\theta_2) + L_3 \cos(\theta_3) &= 0 \\ L_1 \sin(\theta_1) + L_2 \sin(\theta_2) + L_3 \sin(\theta_3) &= L_4 \end{aligned} \quad (13)$$

As this mechanism is harder to intuitively interpret, solving the system from equation 13 is required to find the kinematic relations. As the length of \vec{R}_4 also functions as

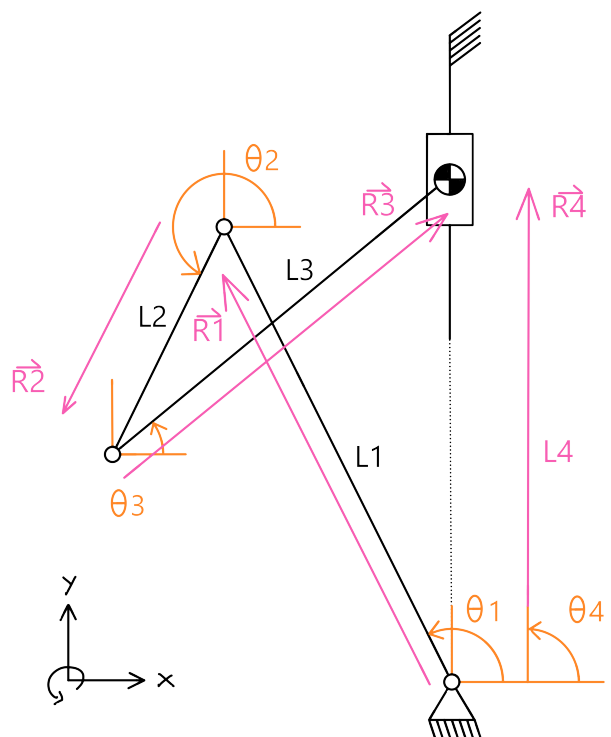


Fig. 5: Revised kinematics

an input, the system can be solved numerically by obtaining the starting angles for a given configuration of θ_1 and $|R_4|$. This would require rebuilding the system in a 3D modeling software like SolidWorks to find these initial angles. SolidWorks also features the function to create angle-plots, and since the system would have to be built in SolidWorks anyway, this method was selected instead to find the kinematic relations instead. After post-processing the raw SolidWorks angle data, figure 6 was derived.

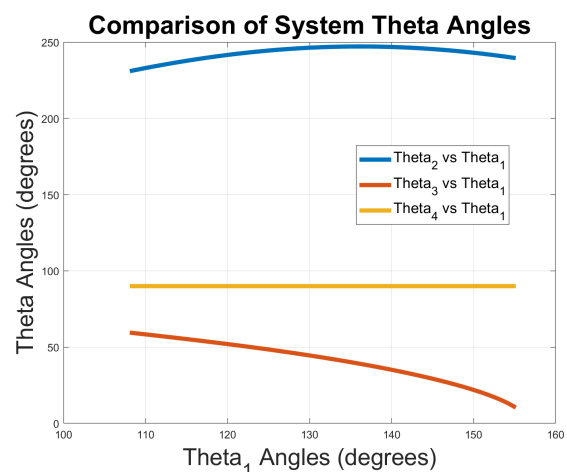


Fig. 6: System Angle Development

TABLE V: System Variables

Angle	Min Angle	Max Angle	Range
θ_1	108.1°	155.1°	47.05°
θ_2	230.99°	247.17°	16.18°
θ_3	10.29°	59.50°	49.21°
θ_4	90.00°	90.00°	0.000°

Table XI shows that the angle ranges of the kinematic solution from figure 5 are suitable to model using the PRBM method as the angle ranges stay below 60°, angle ranges are also visualized in figure 6.

Realizing Jump Directionality

Design requirement FUNC-07 states that the Jumper should be able to be steerable in its jumping direction. Adding traditional steering methods like gyroscopes or tilting feet would over-complicate the design. It was therefore set as an objective to achieve steerability using only one actuator. This actuator would harness a non-linearity in leg stiffness to shape the net-jumping moment of each leg as a function of the actuator displacement.

This was made possible by an increase in the stiffness of different legs for different displacements. This results in a specific leg producing more force for a certain actuator displacement. To achieve control over the direction, a metric governed by the net jumping moment contributed by each leg, would have to be carefully shaped to fit the desired profile. The goal was to create a system that could make the robot jump straight for a low actuation displacement. For a moderate displacement, the robot would jump at angle range *B*, engaging the first two legs. And finally, for a high actuation displacement, when all three legs are engaged, the robot would jump at angle range *C*.

As each leg would be stiffer than the previous one, and therefore generate more force, a delay was introduced, that could split the jumping angle-displacement plot in those three desired regions of displacement.

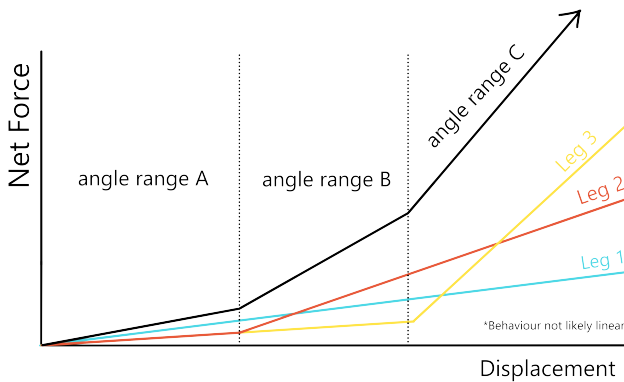


Fig. 7: Angle ranges as a result of delayed leg effects

This delay was realized by providing Leg 2 and Leg 3 with a parallel linkage flexure, functioning as a sort of mechanical delay. For the first region of actuation, the displacement simply flexes the "delay-slider". After a certain offset, the slider hits a break, allowing the elbow to start flexing and functioning as the main contributor to the jumping force.

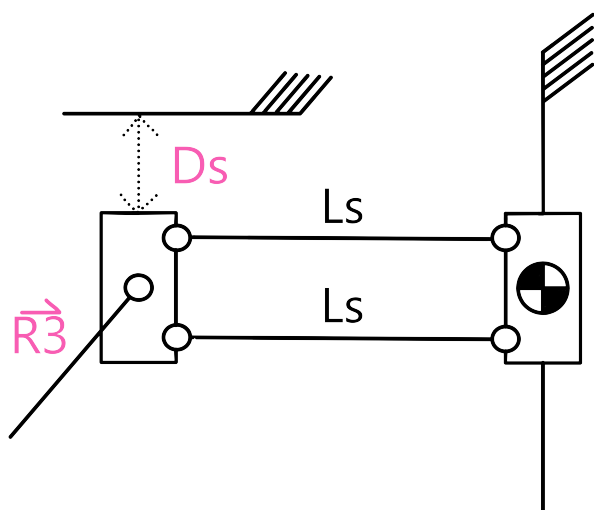
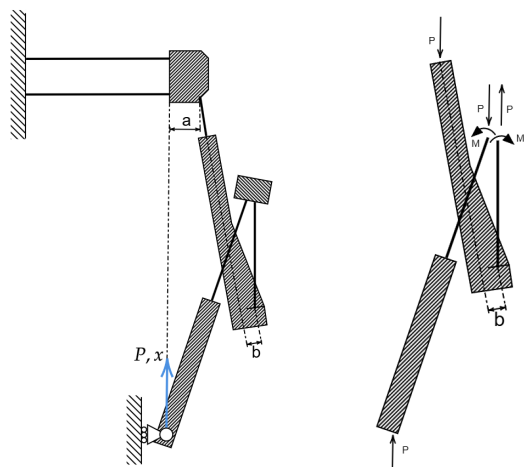


Fig. 8: Kinematics of Slider

Parameters Slider Length *Ls* and Slider Displacement *Ds* can be varied to obtain the desired force-displacement plot for legs 2 and 3. Leg 1 does not feature an offset. Another advantage of this delay system is that the kinematics are not particularly affected. The added mechanism is a parallel linkage, therefore keeping the leg hip connection perfectly vertical. Besides, when the slider reaches the delay, the previously derived kinematics take over again.

Dimensioning and PRBM

The complete leg system was transformed in a Pseudo-Rigid Body Model for the dimensioning step of the design process. First, a schematic representation of the compliant model was obtained (Figure 9a). To simplify the PRBM calculations, the horizontal width of the slider body (*a* in figure) was assumed to be 0, as well as the thigh-upward flexure offset (*b* in figure). The hip small-length flexure was directly modeled as a hinge-spring pair, vertically aligned to the feet, and its stiffness was used as a tunable parameter. Furthermore, the median solid piece that connects the two knee flexures was assumed to be horizontal.



(a) Compliant schematic of (b) Force-moment end loading of leg assembly knee flexures

Fig. 9

The boundary conditions for the remaining flexures are then:

- Slider flexures: fixed - guided
- Upward knee flexure: fixed - fixed
- Downward knee flexure: fixed - fixed

According to [9], each slider flexure was substituted by 2 hinge-spring pairs, and three rigid links. For what concerns the knee flexures, these are subject to a combined force-moment loading (Figure 9b). The 3R model was then chosen, with 3 hinge-spring pairs and 4 rigid links for every body.

The resulting complete PRBM model is shown in Figure 10.

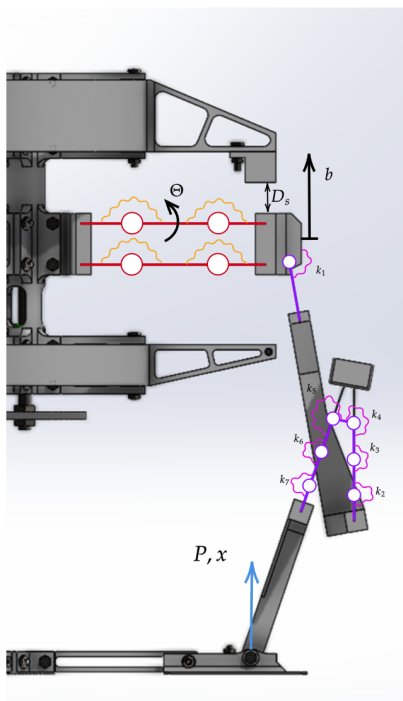


Fig. 10: Full leg assembly PRBM model

Springs $k_1, k_2, k_3, k_4, k_5, k_6$ and k_7 are highlighted, since their 7 hinges constitute the main challenge of the entire PRBM. The 3R model is, in fact, more precise but also more complex than its 2 hinges approximation.

The full model can be seen as a series connection of two translational springs: the slider's flexures and the leg. Vertical force P was considered to be the only transmitted component, and the PRBM solution was split in two.

First, the Force/Displacement function for the slider was obtained:

$$P_s(b) = \frac{4K_\Theta EI\Theta(b)}{l^2 \cos(\Theta(b))} = \frac{4K_\Theta EI \sin^{-1}(\frac{b}{\gamma l})}{l^2 \cos(\sin^{-1}(\frac{b}{\gamma l}))} \quad (14)$$

where: $K_\Theta = 2.654855$

$\gamma = 0.852144$

$l = L_s$ = length of flexures

Note that spring k_1 also transmits a moment on the slider. This was assumed to be negligible for what concerns it's (buckling) effect on the horizontal flexures and their

PRBM. Later testing revealed this not to be completely true (see Sec. Discussion).

The leg part of the leg assembly (highlighted in purple in Figure 10) proved to be more complex. Grounding the slider ($b = 0$) leads to a 6 DoFs system, that had to be solved through energy equations. In particular, Lagrange's static equilibrium equations were used.

For a static equilibrium case, potential energy V and generalized force \underline{Q} are the only term in the equations. Potential energy was computed as

$$\begin{aligned} V = & \frac{1}{2}k_1(q_1 - q_{0_1})^2 + \frac{1}{2}k_2(q_2 - q_1 - (q_{0_2} - q_{0_1}))^2 + \dots \\ & + \frac{1}{2}k_3(q_3 - q_2 - (q_{0_3} - q_{0_2}))^2 + \frac{1}{2}k_4(q_4 - q_3 - (q_{0_4} - q_{0_3}))^2 + \dots \\ & + \frac{1}{2}k_5(q_5 - q_4 - (q_{0_5} - q_{0_4}))^2 + \frac{1}{2}k_6(q_6 - q_5 - (q_{0_6} - q_{0_5}))^2 + \dots \\ & + \frac{1}{2}k_7(\phi_7(\underline{q}) - q_6 - (\phi_7(\underline{q}_0) - q_{0_6}))^2 \end{aligned} \quad (15)$$

where q_i refers to the orientation of the i^{th} link, starting from the hip, and q_{0_i} refers to its fabrication angle. The angle of the last link, ϕ_7 is not a degree of freedom, and was therefore computed as a function of the other angles, \underline{q} .

The generalized force was computed as

$$\underline{Q}(\underline{q}, P) = P \frac{\partial y_p}{\partial \underline{q}}(\underline{q}) \quad (16)$$

where y_p is the vertical coordinate of the end effector, i.e. the application point of force P .

Lagrange's equations are then:

$$\frac{\partial V}{\partial \underline{q}}(\underline{q}) = \underline{Q}(\underline{q}, P) \quad (17)$$

Solving this system for various force inputs P returns points $(P, x = y_p(\underline{q}))$ from the Force/Displacement curve of the leg.

The system was solved numerically, and because of the many possible equilibrium configurations, proved to be quite unstable. That is, the solver would converge and find a numerically correct solution, but said solution would not be a realistic configuration of the system. This was solved by setting the initial force of every force step to the previous step's solution, effectively simulating the real deformation process.

The computed Force/Displacement points where then interpolated using a fitted polynomial $P_l(x - b)$ (Figure 11), in order to generate a proper function that could be utilized with the slider's function $P_s(b)$.

In order to solve the *series springs + offset stopper* configuration, the total displacement for which contact between the slider and its stopper happens, x_c , was first computed. Up until such a displacement, the two springs are in series, meaning that they transmit the same force:

$$P_s(b(=D_s)) = P_l(x_c - b(=D_s)) \quad (18)$$

where $b = D_s$ expresses the contact condition.

Having computed x_c , a Force/Displacement curve for the whole leg assembly can be derived:

$$P(x) = \begin{cases} P_s(b) \text{ with } b | P_s(b) = P_l(x - b) & \text{for } x < x_c, \\ P_l(x - D_s) & \text{for } x \geq x_c, \end{cases} \quad (19)$$

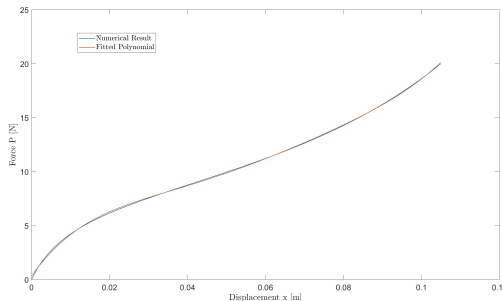


Fig. 11: Polynomial fitting of numerical solution

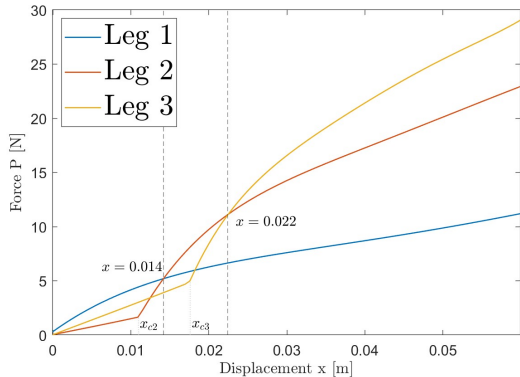


Fig. 12: Tuned Force/Displacement curve for each leg

Note how for the first leg, which has no delay ($x_c = D_s = 0$) the Force/Displacement curve simply becomes $P_l(x)$.

Having obtained the full F/D curve, the three legs were dimensioned (Table XII) in order to maximize the dominance of each leg in its activation zone (see Figure 7). The resulting curves are shown in Figure 12:

For a charging displacement $0 < x < 14\text{mm}$, leg 1 would be the most powerful, and the jump would be in its (opposite) direction. Similarly, for $14\text{mm} < x < 22\text{mm}$ and $22\text{mm} < x$, legs 2 and 3 would take over, and steer the jump in their respective (opposite) direction.

For what concerns the jump calculations, either an energetic or a dynamic approach could have been taken. Given the complexity of the entire Jumper, and the focus of this project on compliant mechanisms, the first, more simplistic, approach was chosen. This meant simply equating the stored energy to the potential energy at peak jump height, neglecting all losses:

$$mgh = \int_0^x P_1(s) + P_2(s) + P_3(s)ds \quad (20)$$

where x is the charging displacement imposed on the legs.

Mass was set at $m = 1\text{kg}$, and the height goal was set at 90cm . The stored energy (in terms of jumping height) and the number of tuned flexures needed to jump the height goal were plotted as a function of the charging displacement:

Figure 13 shows that, in order to achieve the desired jumping height, the stored energy would need to be increased by a factor of 4.3, for example by adding four parallel flexures to every single flexure in the model, or increasing their width.

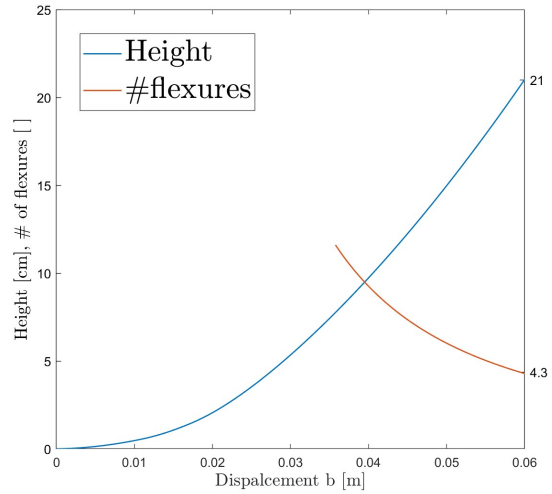


Fig. 13: Stored energy and necessary flexures

Considering the already large size of the tuned legs (see Table XII), the fabrication specifics were left untouched, as calculated through the PRBM, knowing that the jumping height would be limited to around 20cm .

For what concerns the dimensioning of the hip, the cantilever beam with a force at the free end model was used. This was done for simplicity, even though the hip is subject to both a force and a moment, theoretically requiring its own 3R model. Note that the small length flexural pivot model would also be invalid, since the length of the hip flexure is larger than a tenth of the connected link (upper leg). This approximation was knowingly made, and experimental testing was used to calculate the effective stiffness of the hip joint.

Prototype and Test Setup

Conducting measurements is a vital part of design verification. Due to the intricate nature of the leg design, two tests had to be conducted. Test one aimed to measure the effective stiffness of just the elbow joint. Its results would both validate the PRBM approximation and provide effective stiffness values for each elbow joint to be used in simplified PRBM models. Empirically obtained effective elbow stiffness could replace its numerical approximation to refine the used models.

The first test featured a special hinge that allows for free rotation, therefore only plotting the stiffness of the elbow. Figure 14 shows the setup including used tools. The second test introduced the hip joint and delay slider to the test and aimed to measure the actual force response of the leg assemblies. The stiffness of the hip and slider flexures does contribute to the total force response of each leg and should be determined accordingly. As both Leg 2 and 3 featured delay sliders, an additional support structure was required. This support was placed at a distance equal to the delay distance away from the slider at rest and mimicked the effect of the slider stopper.

The components marked in figure 14 and 15 relate to the following:

- **Yellow:** Measurement stage and projected direction
- **Cyan:** Support structure

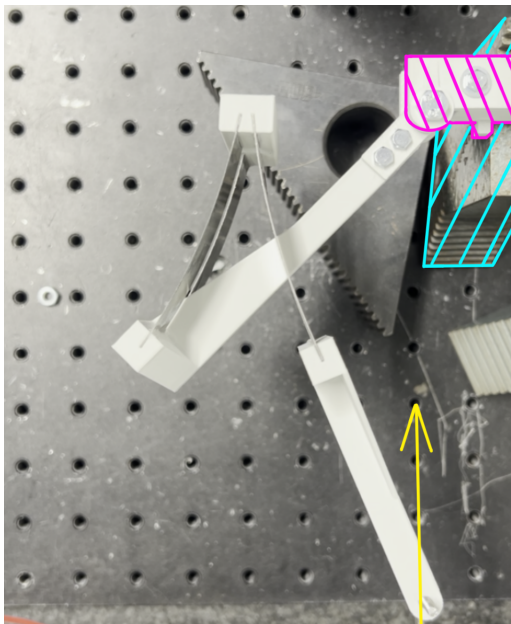


Fig. 14: Test Setup for Effective Elbow Stiffness

- **Pink:** Rotating hinge
- **Red:** Delay support

Note that in figure 15, the support structure is located outside of the figure.

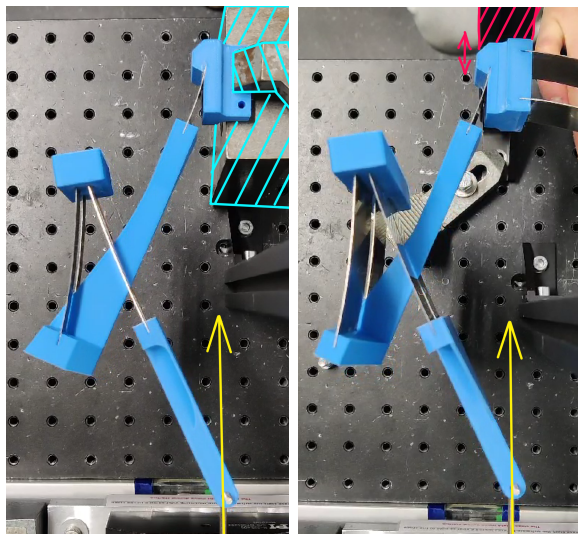


Fig. 15: Test setup for second test

Both tests were executed in a similar fashion, of which the steps are listed below:

- 1) **Align test rig:** Use a rectangular spacer to properly align the measurement stage with the test bed
- 2) **Build support:** Use available build blocks to create the support holding the hip or slider attachments
- 3) **Align supports:** Use a ruler combined with a level gauge to align the hip or slider vertically with the stage. Repeat for vertical alignment. Alignment should replicate the PRBM
- 4) **Secure support:** After alignment, the supports may be secured in place
- 5) **Zero force:** Remove any pre-load on measurement stage by moving it to the zero-force position

6) **Test displacement limits:** Test limits of displacement range by moving the stage to increasing position, reaching the desired maximum range

7) **Conduct measurement:** Move stage back to zero-force position. After increasing resolution, move to maximum range and back to collect data

For a complete list of used tools, please refer to Appendix section C.

Both tests were executed to obtain certain values pertaining to identified performance criteria as identified in section A. Table VI shows these criteria, together with their desired test performance.

TABLE VI: Relevant Performance Metrics

Metric	Desired Function	Desired Values
FUNC-01	The Legs are reusable	10 cycles
FUNC-04	The Jumper releases the stored energy to jump	T or F
FUNC-06	The Jumper is steerable in jumping direction	Force step-up in F/D plot
COND-02	Jumper stores energy by means of compliant mechanics	n.a.

FEM

For the FEM Analysis, Ansys Mechanical 2024 was used. To get the best result the model must be as close to real life as possible. Therefore, a STEP-file of the model was imported and the parts were assigned their relevant material, leaf springs structural steel and printed parts PLA. Large deflections was used to simulate the nonlinearity of the model. In figure 16 the boundary conditions of the static structural analysis are visible. At A (purple surface) there is a fixed support, and at B (yellow arrow) there is a forced displacement in the upwards direction. At point A a force probe was placed to be able to measure the resulting force in the relevant direction. The FEM was done in 20 steps to be able to clearly see the nonlinearity and make a realistic plot. For convergence, the Ansys standard allowable change of 20% was used. This value was chosen arbitrarily and will be validated with the test prototype. A relatively dense mesh with program controlled element order and sizing of 2mm was chosen, resulting in 33538 nodes and 14038 elements. This will also be validated with the test prototype. Next to this flexure, the other legs with the 2x10mm and 2x40mm springs were also simulated. For more details see Appendix I-I.

EXPERIMENTATION AND RESULTS

After a rigorous design campaign, the final model was derived. Figure 17 shows the integrated prototype. Due to the intricate nature of the jumping mechanism, several additional components had to be added. Note that this prototype only aims to demonstrate the mechanics of the Jumper. The actuator is operated manually, and the model does not feature any of its payload/ electrical capabilities. In Figure 18, a closer look can be taken at the working principle. The Actuator Vertical Support ensures a strictly vertical force on the end effector. In the end this force was slightly offset to include a horizontal component due to stabilization concerns. The payload bay structure doubles as the Displacement Stoppers and offer additional leg

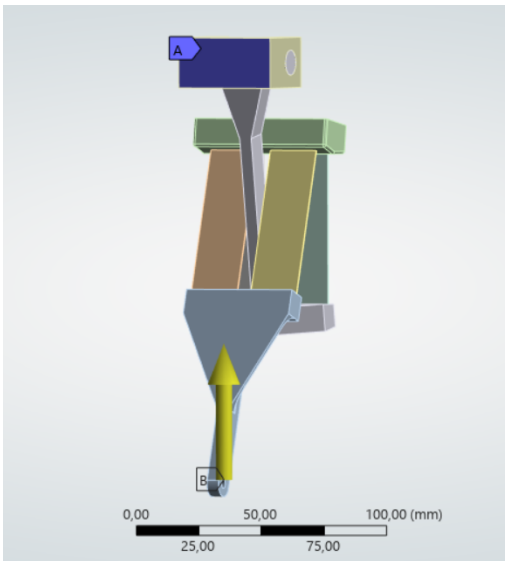


Fig. 16: Ansys model

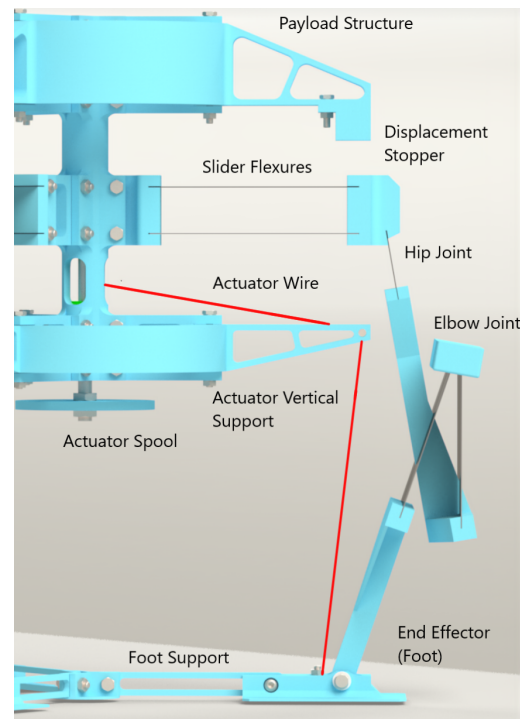


Fig. 18: Final Model Components

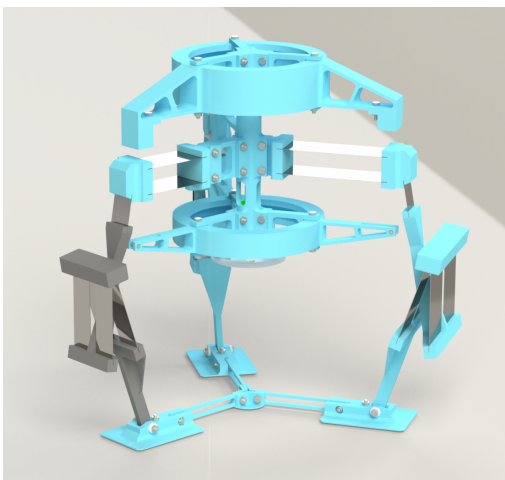


Fig. 17: Final Model

protection. The single Actuator Spool is hidden inside of the main core tree and connects individual actuator wires to each end effector. Lastly, the removable Foot Support connect the feet together to further improve stability.

Two different Force/Displacement tests were carried out. As previously described (see Sec. Prototype and Test Setup) the first test did not involve the slider nor the hip flexure. The latter was replaced by an hinge, whose friction contribution was neglected in FEM and PRBM computations.

Figure 19 shows the comparison results of leg 2 between the PRBM, FEM and measurement. The comparison plots for Leg 1 and 3 can be found in Appendix section I-J.

On top of the numeric comparison, a visual comparison was also carried out. In particular, the deformed configuration computed through the PRBM model was overlayed I-K on a video capture of the experimental test [8].

During the second test, the full leg assembly, complete with slider and hip hinge, was tested. The results (Figure 20) show that the use of the cantilever beam with a force at the free end model (see Sec. PRBM) leads to a hip flexure that is significantly less stiff than its hinge model. Again, the results for leg 1 and leg 3 can be found in Appendix

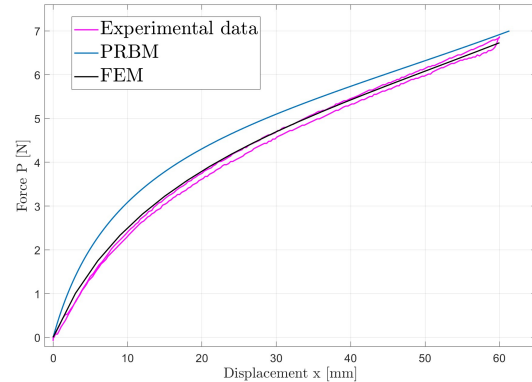


Fig. 19: F/D curves comparison, leg 2, test 1

I-L.

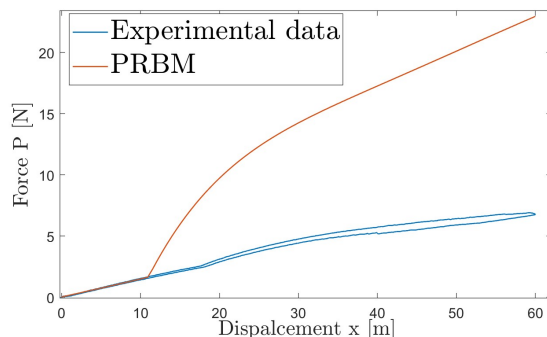


Fig. 20: F/D curve comparison, leg 2, test 2

During the second's leg test, buckling was observed for high charging displacements:

Conclusively, the prototype's performance can be gauged by evaluating to what extend it fulfilled the set design

Criterion	Requirement	Desired Value or Metric	Obtained Value
PROD-01	Horizontal traversal	0.5	+0.095m
PROD-02	Continuous jumping	Self-charging	Manual actuation
PROD-03	Vertical traversal	1 m	+0.10 m
FUNC-01	Reusability	10 cycles	10 cycles (so far)
FUNC-02	Charges self or by human	Both	Only human operated
FUNC-03	Storing mechanical energy	4.91 J	0.774 J
FUNC-04	Releasing energy to jump	61.5 N	10 N
FUNC-05	Protects equipment	Payload and components	Dedicated protective structures
FUNC-06	Steerability	Varying net-force per displacement	Varying net-force per displacement
COND-01	Payload mass	0.5 kg	0.29 kg
COND-02	Uses compliant mechanics	n.a.	Achieved
COND-03	Space grade materials	Teflon, Stainless Steel	PLA, Stainless steel

TABLE VII: Achieved Functionality

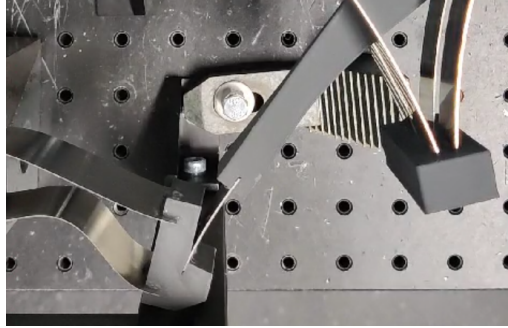


Fig. 21: Buckling mode of second slider

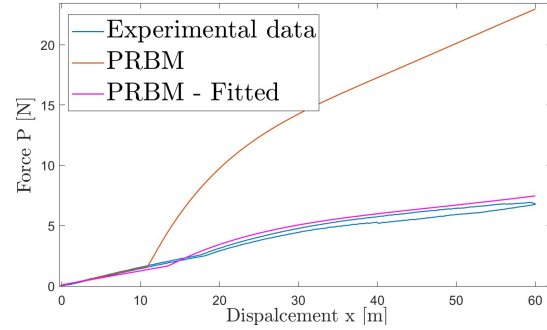


Fig. 22: F/D curve fitting, leg 2, test 2

requirements and performance metrics. Note that the goal of the prototype is to demonstrate the core functionality. For example, the model not being able to perform self-charging is not considered a failure.

DISCUSSION

The results of the two testing sessions were analyzed, in order to validate the PRBM and FEM.

For what concerns the first test, the F/D curves comparison (Figure 19) shows good accuracy on both the PRBM and FEM results, especially considering the complexity of the PRBM model. This accuracy also validates the assumptions made in the FEM analysis. The overlay of the computed deformation on the visual recordings also shows good accuracy with respect to the experimental deformation. The PRBM model of the elbow was therefore considered valid.

For what concerns the second test, involving the full leg assemblies, the experimental data showed relevant discrepancies with the PRBM Force/Displacement curves. This is to be expected, as the PRBM model chosen for the hip flexure is an approximate solution, to be corrected through testing. As can be seen in Figure 20, the hip proved to be considerably less stiff than what had been predicted, with the PRBM curve showing much higher force for equal displacement. Nonetheless, the second test validates the slider flexure's PRBM model, that follows the experimental data very well (Figure 43 and 44) up until the PRBM's contact displacement.

The PRBM was then fitted, by tuning of the effective hip stiffness k_1 , to the experimental data (see Figure 22). The refitted PRBM for legs 1 and 3 can be found in Appendix section I-M.

Note that, even though refitted, the PRBM's F/D curves do not follow the experimental data as close as the first

test (see Figure 19). This can be attributed to the simplistic one hinge model chosen for the hip flexure, that, even with backward tuning, cannot accurately capture the behavior of a fixed-fixed flexure.

The effective stiffness found through the fitting process is shown in Table VIII:

Parameter	Leg 1	Leg 2	Leg 3
PRBM's k_1	0.90 Nm/rad	2.28 Nm/rad	2.28 Nm/rad
Effective k_1	0.12 Nm/rad	0.14 Nm/rad	0.14 Nm/rad

TABLE VIII: Tuned PRBM parameters

The complete PRBM was then updated with these new-found values, to estimate the new F/D curves and jumping height. The results are shown in Figure 23 and 24.

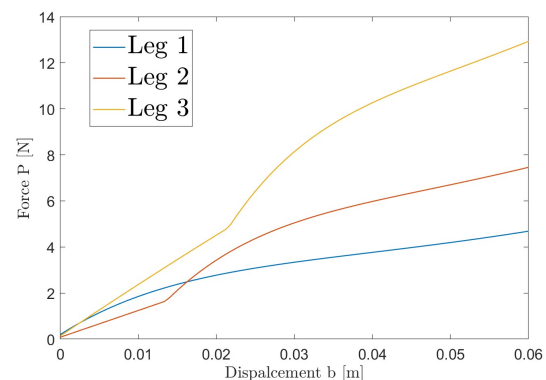


Fig. 23: Retuned F/D curve for each leg

The refitted PRBM shows a loss of steerability in the model, due to the third leg always being the peak contributor. This was also observed when testing the full

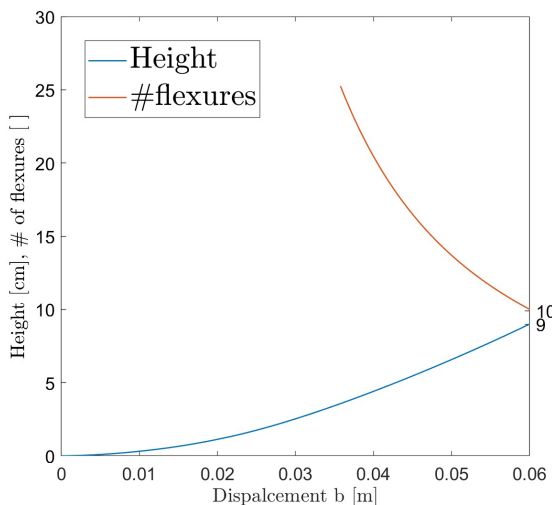


Fig. 24: Stored energy and necessary flexures after retuning

prototype, that upon charging would always jump in the same direction, away from the third leg (see Figure 49).

Decreasing the stiffness of the hips in the PRBM also led to a considerable decrease in the stored energy (Figure 24), with a predicted jumping height of 9cm for a 60mm charging displacement. This value also proved to be accurate when testing the full prototype (see Figure 48).

Furthermore, experimental testing showed that upon fully charging the prototype, the second leg's slider would buckle (figure 21). Though a sign of non-negligible moment exerted by the hip, this buckling does not have a completely invalidating effect on the final Force/Deflection PRBM plot. The buckling, in fact, only happens at a late stage in the charging process, when the slider is already in contact with its hard stop, and the force through the leg is mostly due to the deformation of the leg itself. The only change in the energy stored in the leg is due to the drop in the torsion of the hip spring. This behavior also explains the hysteresis exhibited by the second leg (see 22).

The next step in the dimensioning of a next prototype would be achieving the desired F/D curves for all the legs, in order to render the prototype steerable through single actuator. Two approaches could be taken:

- Further PRBM enhancement: introducing the 3R model for the hip would bring the same accuracy of the validated elbow joint PRBM, leading to a one-shot tuning and dimensioning process.
- Iterative refinement: adapting the hip's flexure dimension, having seen the effective stiffness of the previous iteration, could quickly bring the specifications to a satisfying level.

Besides the force deficit being the leading cause for the failure to achieve the performance metrics, the other main cause is likely the increased mass. As the original mass was set to 0.5 kg, the additional 0.29 kg increased the energy needed to jump as PROD-03 dictated increased too.

Improving the jumping performance comes down to maximizing the jumping work performed (Equation 1) and minimizing mass. Decreasing mass can thus be achieved by better integrating system components, like using the same

structure for both the Displacement Stopper and Vertical Support. Deriving an actuation scheme consisting of less components in general will also directly lower system mass. Thirdly, using novel materials like CFRPs may further assist in reducing mass. Increasing the work function comes down to further tuning the PRBM, balancing flex range (and thus end-effector path length s) and deliverable force F . Novel materials could also play an important role in PRBM tuning and leg part design, allowing the legs to generate more force.

CONCLUSION

This report documented on the design process of a compliant Martian exploration vessel. After careful kinematic synthesis, the mechanism was turned compliant using numerical methods which were in turn verified using measurement and FEM data. The result of the kinematic analysis yielded a promising solution to an otherwise conventional mechanism, one that would push the limits of compliant mechanism design. It combined principles from classical spring mechanics to overcome the "stiffness versus flexibility" problem. Due to its intricate nature, challenging numerical models were built to analyze the system's behavior. After verifying the PRBM model using FEM data and measurement tests, the design was further optimized, striving to achieve its functionality. Iteration played a key role in the design process, and the adaptability of the PRBM model proved to be very helpful. Discrepancies between the prototype's behavior and numerical model were tracked and implemented and suggestions on how to improve the model were made accordingly. Future work on this specific prototype would focus on optimizing the mass distribution, end-effector path and PRBM tuning. Novel, lightweight materials could play an important role in allowing for stronger flexures while not comprising any component strength. Furthermore, remotely operated actuator systems would allow the system to achieve its fully-autonomous operation cycle.

Despite not achieving its full-functionality, especially the requirements relating to jump height, the project proved that compliant mechanisms can elevate the design space for extra-terrestrial exploration.



Fig. 25: Jumper posing in the workshop

ACKNOWLEDGEMENT

We would like to cordially thank Davood Farhadi for helping us out countless times and providing the much needed technical expertise, Mats de Jong for helping us execute the first measurement test and Eelco Kleiman for allowing us to conduct our third last-minute test.

ADDED MATERIAL CONTENTS

References	13
-------------------	----

I Appendix	14
I-A Weighted Criteria table	14
I-B SolidWorks Assemblies for mechanism synthesis	14
I-C Kinematic Linkage Parameters	15
I-D Stiffness versus Flexibility Problem and Solution	16
I-E SolidWorks Angle Plots	17
I-F Measurement Test Tools	17
I-G PRBM Matlab Code	18
I-H PRBM Dimensioning Values	25
I-I Ansys FEM	25
I-J First Test Elbow Stiffness Results	28
I-K First Test Video Overlay	30
I-L Second Test Results	31
I-M Second Test PRBM retuning	33
I-N Jump Test	35
I-O Symposium Presentation Slides	36

REFERENCES

- [1] Savu, G. (2006). Earth-Mars similarity criteria for exploring martian vehicles. *Acta Astronautica*, 59, 8-11, pages 734-741. <https://doi.org/10.1016/j.actaastro.2005.07.001>
- [2] Ouyang, P.R., Tjiptoprodjo, C., Zhang, W.J., Yang G.S. (2006). Micro-motion devices technology: The state of arts review. *The International Journal of Advanced Manufacturing Technology*, 38, 463-478. <https://link.springer.com/article/10.1007/s00170-007-1109-6>
- [3] Howell, L. L. (2012). Compliant mechanisms. In Springer eBooks (pp. 189–216). <https://doi.org/10.1007/978-1-4471-4510-37>
- [4] Brandt Sasiharan Elias Mhatre 2021, Jump takeoff in a small jumping Spider - Journal of Comparative Physiology A, <https://link.springer.com/article/10.1007/s00359-021-01473-7>, Brand, Erin E. and Sasiharan, Yoshan and Elias, Damian O. and Mhatre, Natasha, y
- [5] The energetics of the jump of the locust *Schistocerca gregaria*, <https://journals.biologists.com/jeb/article/63/1/53/22130/The-energetics-of-the-jump-of-the-locust>, Journal of experimental biology, H. C. Bennet-Clark, 1975, August
- [6] Design Exploration and Kinematic Tuning of a Power Modulating Jumping Monopod, <https://par.nsf.gov/servlets/purl/10025795>, Mark M. Plecnik
- [7] Jumping kinematics in the wandering spider *Cupiennius salei*, <https://link.springer.com/article/10.1007/s00359-010-0527-3>, Tom Weihmann
- [8] Henriques, J. Figure to play and analyze videos with custom plots on top. *MATLAB Central File Exchange*. Retrieved from <https://www.mathworks.com/matlabcentral/fileexchange/29544-figure-to-play-and-analyze-videos-with-custom-plots-on-top>.
- [9] Lusk, C. (2013). *Handbook of Compliant Mechanisms*. John Wiley and Sons, Ltd. Retrieved from <https://onlinelibrary.wiley.com/doi/abs/10.1002/9781118516485.ch5>.

I. APPENDIX

A. Weighted Criteria table

	Weight	Triangle	Triangle total	Spider	Spider total
Reliability	9	4	36	3	27
Power/Weight	8	3	24	5	40
Precision	3	3	9	4	12
Weight	6	2	12	3	18
Compliance	5	3	15	3	15
Size	3	1	3	3	9
Total			99		131

Fig. 26: Evaluated concepts

B. SolidWorks Assemblies for mechanism synthesis

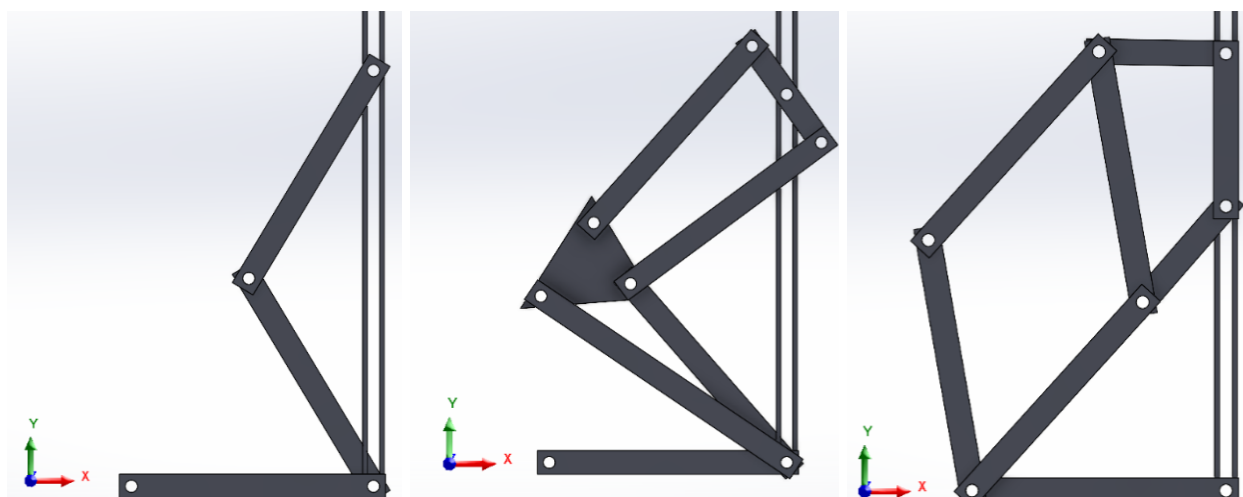


Fig. 27: Mechanism 1, 2 and 3 Test Assembly

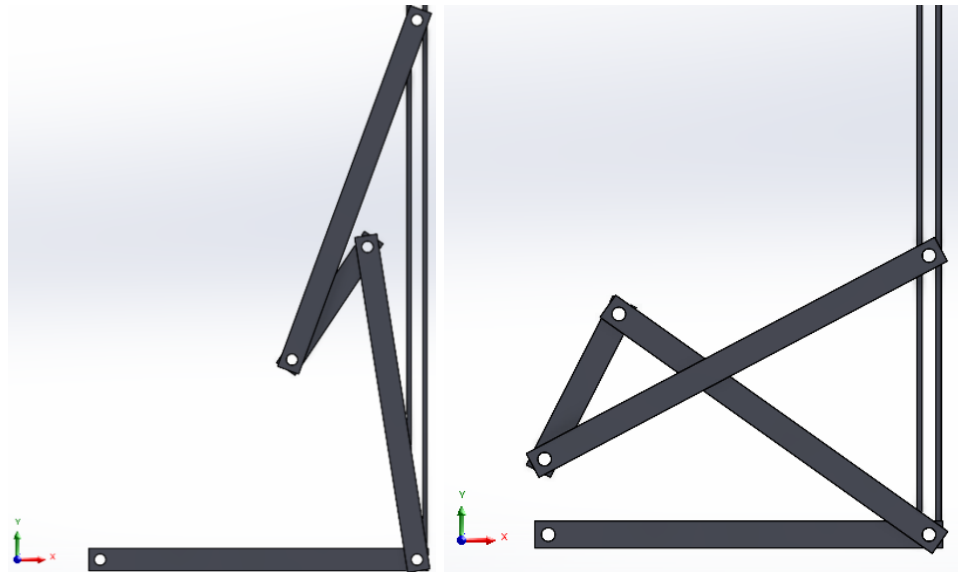


Fig. 28: Fabrication- and operation angle of mechanism

C. Kinematic Linkage Parameters

TABLE IX: Linkage 1 Parameters

Variable	Status	Value
L1	Known, constant	100mm
θ_1	Known, input	$\frac{pi}{1} \text{ to } \pi \text{ rad}$
L2	Known, constant	100mm
θ_2	Unknown	rad
L3	Unknown	mm
θ_3	Known, constant	$\frac{\pi}{2} \text{ rad}$

TABLE X: Final Linkage Parameters

Variable	Status	Value
L1	Known, constant	140mm
θ_1	Known, input	$[108.1^\circ \quad 155.1^\circ] \text{ rad}$
L2	Known, constant	60mm
θ_2	Unknown	rad
L3	Known, constant	130mm
θ_3	Unknown	rad
L4	Known, input	$[224.3\text{mm} \quad 35.75\text{mm}]$
θ_4	Known, constant	90°

D. Stiffness versus Flexibility Problem and Solution

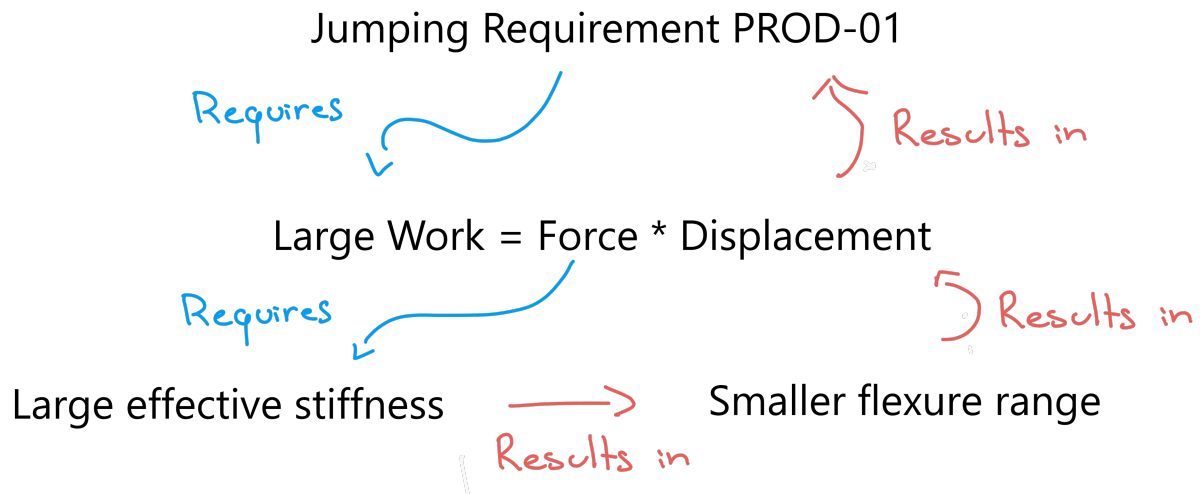


Fig. 29: The Stiffness versus Flex range problem



Fig. 30: Proof of concept model

E. SolidWorks Angle Plots

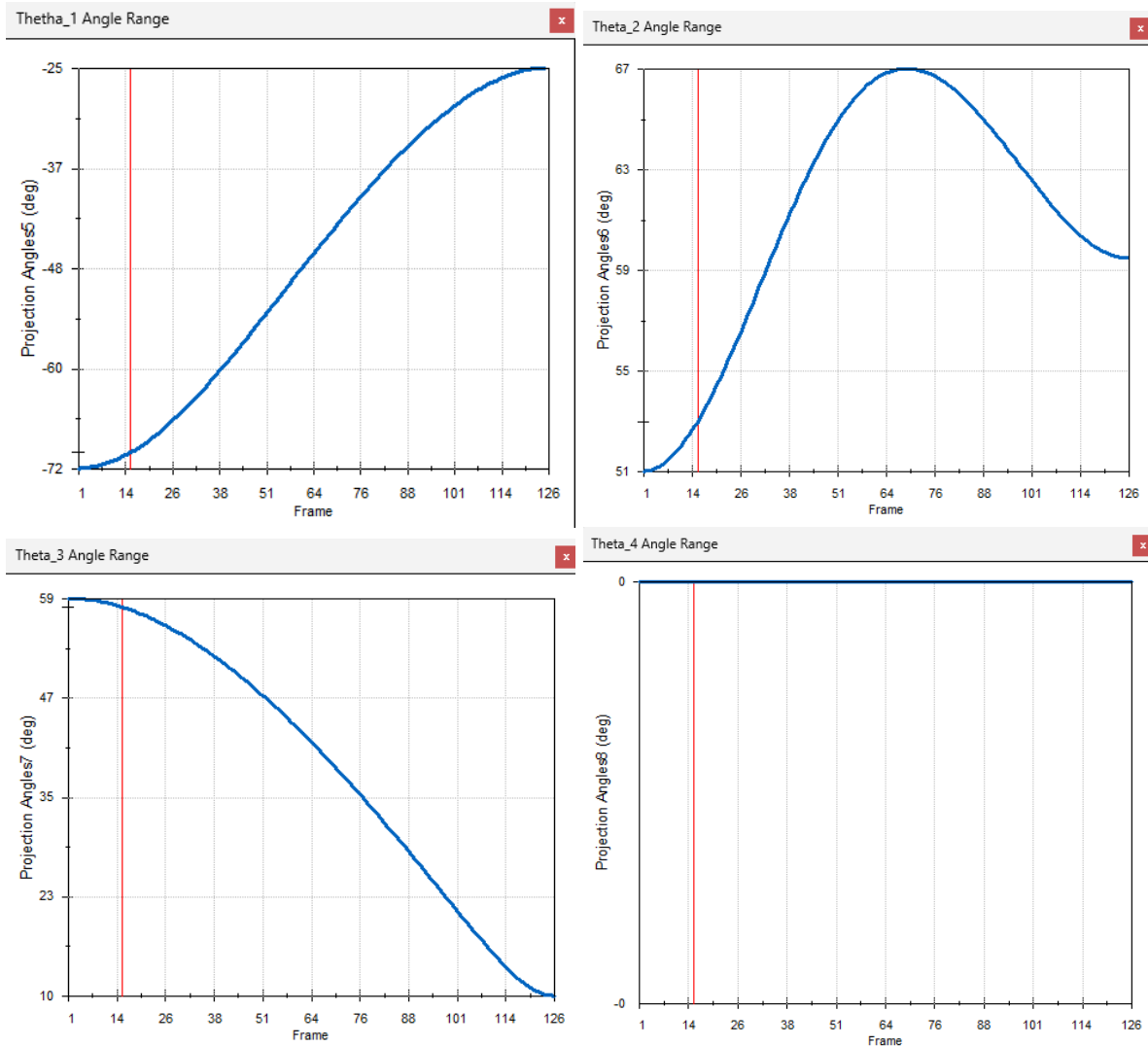


Fig. 31: SW Theta Angle Plots

F. Measurement Test Tools

TABLE XI: Measurement Test Required Tools

Tool	Amount
Test Bed	1
Support Blocks	2 pairs
Support Clamps + Rod	2
Displacement Stopper	1
Leg Specimen	3 + 3
Camera Stand	1
Measurement Stage	1
Rectangular Spacer	1
Computer	1
Wrench Set	1
Level Gauge	1
Ruler	1

G. PRBM Matlab Code

Below the main PRBM.m code used in the PRBM calculations. Many of the plots in this document were obtained through different versions of this code. Contact f.p.milazzo@student.tudelft.nl for these (or don't).

```
%% PRBM for the new, non-curved model

clc
clear
close all

%% Code setup

%% Variables
% Given:
E = 190e9; % Young's modulus
h_20 = 0.00015; % Thickness of second slider flexures
h_30 = 0.0003; % Thickness of third slider flexures
gamma = 0.852144; % PRBM coefficient
K_t = 2.654855; % PRBM coefficient

% Customizable:
mass = 1;
height = 0.9;
energoal = mass*9.81*height;

% Elbows setup (equal geometry for the 3 legs)
l_up = 0.10; % length of the upper leg
l_down = 0.08; % length of the lower leg
l_flex_up = 0.06; % lenght of the flexure connected to the upper leg (outmost flexure)
l_flex_down = 0.06; % lenght of the flexure connected to the lower leg (inmost flexure)
w_1 = 0.02; % total width of flexures (sum of parallel) on first leg
h_1 = 0.0004; % thickness of elbow flexures on first leg
w_2 = 0.04; % total width of flexures (sum of parallel) on second leg
h_2 = 0.0004; % thickness of elbow flexures on second leg
w_3 = 0.08; % total width of flexures (sum of parallel) on third leg
h_3 = 0.0004; % thickness of elbow flexures on third leg
I_1 = w_1*h_1^3/12; % surface moment of inertia of both flexures on the first leg
I_2 = w_2*h_2^3/12; % surface moment of inertia of both flexures on the first leg
I_3 = w_3*h_3^3/12; % surface moment of inertia of both flexures on the first leg
d = 0.002; % distance between the two flexures on the median solid piece, assumed to be horizontal at fabrication
theta_up = deg2rad(290);

% fabrication angle of the upper leg (absolute angle)
theta_flex_up = deg2rad(100);

% fabrication angle of the flexure connected to the upper leg (outmost flexure) (absolute angle)
theta_flex_down = mod(-acos(-(l_up*cos(theta_up)+l_flex_up*cos(theta_flex_up)-d)/(l_flex_down+l_down)),2*pi); % fabrication angle of the flexure connected to the lower leg (inmost flexure) (absolute angle)
```

```

theta_down = theta_flex_down;

    % fabrication angle of the flexure connected to the lower leg (inmost flexure)
    % (absolute angle)
k1_1 = 0.12;                      % torsional stiffness of the hinge that connects
                                    % first upper leg and slider
k1_2 = 0.14;                      % torsional stiffness of the hinge that connects
                                    % second upper leg and slider
k1_3 = 0.14;                      % torsional stiffness of the hinge that connects
                                    % third upper leg and slider

% Sliders setup
b_2 = 0.01;                        % Displacement after which the second slider hits
b_3 = 0.015;                        % Displacement after which the third slider hits
l_20 = 0.05;                        % Length of second slider flexures
l_30 = 0.08;                        % Length of third slider flexures
assert(l_30>l_20,'l_30 is not longer than l_20, why is that??')
w_20 = 0.03;                        % Width of second slider flexures
w_30 = 0.03;                        % Width of third slider flexures

P_max1 = 20;                         % Newtons, max force first elbow
P_max2 = 30;                         % Newtons, max force second elbow
P_max3 = 30;                         % Newtons, max force third elbow
step1 = 0.05;                        % Step of force in first lagrange solutions
step2 = 0.05;                        % Step of force in second lagrange solutions
step3 = 0.05;                        % Step of force in third lagrange solutions

%% Elbow polynomial coefficients:
p_1 = PRBM_poly(l_up,l_down,l_flex_up,l_flex_down,E,I_1,d,theta_up,theta_flex_up,
                 theta_flex_down,theta_down,k1_1,P_max1,step1);
p_2 = PRBM_poly(l_up,l_down,l_flex_up,l_flex_down,E,I_2,d,theta_up,theta_flex_up,
                 theta_flex_down,theta_down,k1_2,P_max2,step2);
p_3 = PRBM_poly(l_up,l_down,l_flex_up,l_flex_down,E,I_3,d,theta_up,theta_flex_up,
                 theta_flex_down,theta_down,k1_3,P_max3,step3);
TF_elbow = @(x,p) polyval(p,x);

%% PRBM relationships
% I = @(w,h) w.*h.^3./12;          % Moment of inertia
% theta = @(l,b) asin(b/gamma/l);      % PRBM angle
% a = @(l,b) l*(1-gamma*(1-cos(theta(b))));   % Horizontal offset
% k = @(l,w,h_) 2*gamma*K_t*E/l*I(w,h_);       % PRBM stiffness

%% Contact displacements
cont_2 = @(x) TF_slider(b_2,l_20,w_20,h_20,E) - TF_elbow(x-b_2,p_2);
b_2c = real(fsolve(cont_2,0,optimoptions('fsolve','Display','off')));
                                % Displacement b after which slider 2 stops

cont_3 = @(x) TF_slider(b_3,l_30,w_30,h_30,E) - TF_elbow(x-b_3,p_3);
b_3c = real(fsolve(cont_3,0,optimoptions('fsolve','Display','off')));
                                % Displacement b after which slider 2 stops

%% Total forces and energy
TF_total =@(b) TF_elbow(b,p_1)+TF_leg(b,l_20,w_20,h_20,b_2c,b_2,E,p_2)+TF_leg(b,
                                         l_30,w_30,h_30,b_3c,b_3,E,p_3);      % Total force given by the three legs
energy = @(b) integral(TF_total,0,b);                                     %
                                                               % Total energy stored by the three legs

%% Figures

```

```

b_val = linspace(0,0.06);

figure
subplot(2,2,1)
plot(b_val,TF_elbow(b_val,p_1))
hold on
plot(b_val,TF_leg(b_val,l_20,w_20,h_20,b_2c,b_2,E,p_2))
plot(b_val,TF_leg(b_val,l_30,w_30,h_30,b_3c,b_3,E,p_3))
title('Individual forces')
xlabel('Dispalcement b [m]')
ylabel('Force P [N]')
legend('Leg 1','Leg2','Leg3')

subplot(2,2,3)
plot(b_val,TF_total(b_val))
title('Total force')
xlabel('Dispalcement b [m]')
ylabel('Force P [N]')

energy_val = [];
for ii = 1:length(b_val)
    energy_val(ii) = energy(b_val(ii));
end
subplot(1,2,2)
plot(b_val,energy_val)
hold on
plot(b_val(60:end),energoal./energy_val(60:end))
title('Stored energy and necessary flexures')
xlabel('Dispalcement b [m]')
ylabel('Energy [J]')
legend('Energy','#flexures')


figure
plot(b_val,TF_elbow(b_val,p_1))
hold on
plot(b_val,TF_leg(b_val,l_20,w_20,h_20,b_2c,b_2,E,p_2))
plot(b_val,TF_leg(b_val,l_30,w_30,h_30,b_3c,b_3,E,p_3))
title('Individual forces')
xlabel('Dispalcement b [m]')
ylabel('Force P [N]')
legend('Leg 1','Leg2','Leg3')
%%
figure(1)
energy_val = [];
for ii = 1:length(b_val)
    energy_val(ii) = energy(b_val(ii));
end
plot(b_val,energy_val/9.81/mass*100)
hold on
plot(b_val(60:end),energoal./energy_val(60:end))
title('Stored energy and necessary flexures')
xlabel('Dispalcement b [m]',Interpreter='latex')
ylabel('Height [cm], \# of flexures [ ]',Interpreter='latex')
legend('Height','\#flexures')

function p = PRBM_poly(l_up,l_down,l_flex_up,l_flex_down,E,I,d,theta_up,

```

```

theta_flex_up,theta_flex_down,theta_down,k1,P_max,step)

%step = 0.05;      % Newtons, step

P_val = (0:step:P_max)';
b_val = zeros(length(P_val),1);
ii = 0;
fig = figure;
for P = 0:step:P_max
    ii = ii+1;
    if P == 0
        gamma_0 = 0.125;
        gamma_1 = 0.351;
        gamma_2 = 0.388;
        gamma_3 = 0.136;
        q_init = [0, 0, 0, 0, 0, 0]'; % Vector of initial angles of PRBM bars
        q_init(1) = mod(angle(l_up*cos(theta_up) + l1*l_up*sin(theta_up) +
            l_flex_up*cos(theta_flex_up)*gamma_0 + l1*l_flex_up*sin(theta_flex_up)*
            gamma_0),2*pi);
        q_init(2) = theta_flex_up;
        q_init(3) = theta_flex_up;
        q_init(4) = angle(gamma_3*l_flex_up*cos(theta_flex_up)+l1*l_flex_up*
            gamma_3*sin(theta_flex_up) + gamma_3*l_flex_down*cos(theta_flex_down) +
            l_flex_down*l1*sin(theta_flex_down)*gamma_3 -d);
        q_init(5) = theta_flex_down;
        q_init(6) = theta_flex_down;

    end
    [b, S, l, q0] = elbow_solve(P, l_up, l_down, E, I, l_flex_up, l_flex_down, d,
        theta_up, theta_down, theta_flex_up, theta_flex_down, k1,q_init);
    b_val(ii) = b;
    if mod(P,0.5)==0
        %% Plot the shapes
        x_start = 0;
        y_start = 0;
        figure(fig)
        delete(subplot(1,2,2))
        subplot(1,2,2);
        hold on;
        axis equal;
        grid on;
        xlabel('X');
        ylabel('Y');
        title(['Deformed leg for P = ',num2str(P), ' N']);
        for i = 1:length(l)
            x_end = x_start + l(i) * cos(S(i)); % Coordinata X finale
            y_end = y_start + l(i) * sin(S(i)); % Coordinata Y finale
            quiver(x_start, y_start, x_end - x_start, y_end - y_start, 0, 'LineWidth'
                , 2, 'MaxHeadSize', 0.5);
            x_start = x_end;
            y_start = y_end;
        end
        text(0.04,-0.005, ['b = ' , num2str(b*1000), ' mm'])
    end
    if P == 0
        x_start = 0;
        y_start = 0;
        subplot(1,2,1)
        hold on;
        axis equal;
    end
end

```

```

grid on;
xlabel('X');
ylabel('Y');
title('Undeformed leg');
for i = 1:length(l)
    x_end = x_start + l(i) * cos(q0(i)); % Coordinata X finale
    y_end = y_start + l(i) * sin(q0(i)); % Coordinata Y finale
    quiver(x_start, y_start, x_end - x_start, y_end - y_start, 0, '
        LineWidth', 2, 'MaxHeadSize', 0.5);
    hold on
    x_start = x_end;
    y_start = y_end;
end
end

q_init = S(1:6);
end
%%
p = polyfit(b_val,P_val,5);

figure
plot(b_val,P_val)
hold on
plot(b_val,polyval(p,b_val))

%% Function that returns the vertical displacement b, given a certain vertical
%% force P.
% l_up is the length of the upper leg
% l_down is the length of the lower leg
% E is the Young modulus of both flexures
% I is the surface moment of inertia of both flexures
% l_flex_up is the lenght of the flexure connected to the upper leg (outmost
% flexure)
% l_flex_down is the lenght of the flexure connected to the lower leg (inmost
% flexure)
% d is the distance between the two flexures on the median solid piece, assumed
% to be horizontal
% theta_up is the fabrication angle of the upper leg (absolute angle)
% theta_down is the fabrication angle of the lower leg (absolute angle)
% theta_flex_up is the fabrication angle of the flexure connected to the upper
% leg (outmost flexure) (absolute angle)
% theta_flex_down is the fabrication angle of the flexure connected to the lower
% leg (inmost flexure) (absolute angle)
% k1 is the torsional stiffness of the hinge that connects upper leg and slider

function [b, S, l,q0] = elbow_solve(P, l_up, l_down, E, I, l_flex_up, l_flex_down
, d, theta_up, theta_down, theta_flex_up, theta_flex_down, k1,q_init)

assert(theta_flex_down == theta_down,'Why is the lower (inmost) flexure not
aligned with the lower leg??')
assert(abs((l_up*cos(theta_up)+l_flex_up*cos(theta_flex_up)-d+l_down*cos(
theta_down)+l_flex_down*cos(theta_flex_down)))<1e-15,'feet is not at x = 0!!
(1)')

syms q1 q2 q3 q4 q5 q6
q = [q1; q2; q3; q4; q5; q6];
%syms l_up l_down E I l_flex_up l_flex_down d theta_up theta_down theta_flex_up
% theta_flex_down k1

gamma_0 = 0.125;
gamma_1 = 0.351;

```

```

gamma_2 = 0.388;
gamma_3 = 0.136;
K_t1 = 3.25;
K_t2 = 2.84;
K_t3 = 2.95;

k = [k1, 0, 0, 0, 0, 0, 0]; % Vector containing the stiffnesses of the PRBM
springs
k(2) = K_t1*E*I/l_flex_up;
k(3) = K_t2*E*I/l_flex_up;
k(4) = K_t3*E*I/l_flex_up;
k(5) = K_t3*E*I/l_flex_down;
k(6) = K_t2*E*I/l_flex_down;
k(7) = K_t1*E*I/l_flex_down;

l = [0, 0, 0, 0, 0, 0]'; % Vector containing the lengths of the PRBM bars
l(1) = abs(l_up*cos(theta_up) + l_flex_up*sin(theta_up) + l_flex_up*cos(
theta_flex_up)*gamma_0 + l_flex_up*sin(theta_flex_up)*gamma_0);
l(2) = l_flex_up*gamma_1;
l(3) = l_flex_up*gamma_2;
l(4) = abs(gamma_3*l_flex_up*cos(theta_flex_up)+l_flex_up*gamma_3*sin(
theta_flex_up) + gamma_3*l_flex_down*cos(theta_flex_down)+l_flex_down*gamma_3*sin(
theta_flex_down)*gamma_3 -d);
l(5) = l_flex_down*gamma_2;
l(6) = l_flex_down*gamma_1;
l(7) = l_down+l_flex_down*gamma_0;

q0 = [0, 0, 0, 0, 0, 0]'; % Vector of initial angles of PRBM bars
q0(1) = mod(angle(l_up*cos(theta_up) + l_flex_up*sin(theta_up) + l_flex_up*cos(
theta_flex_up)*gamma_0 + l_flex_up*sin(theta_flex_up)*gamma_0),2*pi);
q0(2) = theta_flex_up;
q0(3) = theta_flex_up;
q0(4) = angle(gamma_3*l_flex_up*cos(theta_flex_up)+l_flex_up*gamma_3*sin(
theta_flex_up) + gamma_3*l_flex_down*cos(theta_flex_down)+l_flex_down*gamma_3*sin(
theta_flex_down)*gamma_3 -d);
q0(5) = theta_flex_down;
q0(6) = theta_flex_down;

phi_7 = @(q_) -acos(-sum(l(1:6).*cos(q_(1:6))))/l(7)); % Angle of lower leg

assert(abs(sum(l(1:6).*cos(q0(1:6)))+l(7)*cos(phi_7(q0)))<1e-15,'feet is not at x
= 0!! (2)')

V = 1/2*k(1)*(q(1)-q0(1))^2 + 1/2*k(2)*(q(2)-q(1)-(q0(2)-q0(1)))^2 + ...
1/2*k(3)*(q(3)-q(2)-(q0(3)-q0(2)))^2 + 1/2*k(4)*(q(4)-q(3)-(q0(4)-q0(3)))^2 +
...
1/2*k(5)*(q(5)-q(4)-(q0(5)-q0(4)))^2 + 1/2*k(6)*(q(6)-q(5)-(q0(6)-q0(5)))^2 +
...
1/2*k(7)*(phi_7(q)-q(6)-(phi_7(q0)-q0(6)))^2;

for ii = 1:6
dV(ii,1) = diff(V,q(ii));
end

assert(isequal(size(dV),[6,1]),'dV is not 6x1 as expected!!')

y_p = sum(l(1:6).*sin(q(1:6)))+l(7)*sin(phi_7(q));
for ii = 1:6
Q(ii,1) = diff(y_p,q(ii))*P;

```

```

end
assert(isequal(size(Q), [6,1]), 'Q is not 6x1 as expected!!!')

eq = dV == Q;
sym_fun = dV-Q;
fun = matlabFunction(sym_fun, 'Vars', {q});
q_init = q_init;
S = fsolve(fun,q_init,optimoptions('fsolve','Display','off'));
b = sum(l(1:6).*sin(S(1:6)))+l(7)*sin(phi_7(S)) - sum(l(1:6).*sin(q0(1:6)))-l(7)*
    sin(phi_7(q0));
S = [S;phi_7(S)];
q0 = [q0; mod(phi_7(q0),2*pi)];
%% Function that returns the vertical force P of the offset legs
function P = TF_leg(b_in,l_i0,w_i0,h_i0,b_ic,b_i,E,p)
P = [];
TF_elbow = @(x) polyval(p,x);
for b = b_in
if b < b_ic
    fun_2 = @(x) TF_slider(b-x,l_i0,w_i0,h_i0,E) - TF_elbow(x);
    x_2 = fsolve(fun_2,0,optimoptions('fsolve','Display','off'));%  

        Displacement of second flexure
    P_add = TF_elbow(x_2);
    P = [P,P_add];
elseif b >= b_ic
    P_add = TF_elbow(b-b_i);
    P = [P,P_add];
else
    error('some problem with b_2 and b')
end
end
end

% Function that returns the vertical force P of a slider and it's offset
function [P,a] = TF_slider(b,l_1,w_1,h,E)
%PRBM coefficients:
gamma = 0.852144; % PRBM coefficient
K_t = 2.654855; % PRBM coefficient
%PRBM relationships:
I = @(w,h) w.*h.^3./12; % Moment of inertia
theta = @(l,b) asin(b/gamma/l); % PRBM angle
k = @(l,w,h_) 2*gamma*K_t*E/l*I(w,h_); % PRBM stiffness

%P = (2*k(l_1,w_1,h)*theta(l_1,b)/l_1/gamma); % Vertical force generated
a = (l_1*(1-gamma*(1-cos(theta(l_1,b))))); % Horizontal offset

%P = (2*k(l_1,w_1,h).*theta(l_1,b)./a); % Vertical force generated
P = 4*K_t*E*I(w_1,h)*theta(l_1,b)/l_1^2./cos(theta(l_1,b));
end

```

H. PRBM Dimensioning Values

Parameter	Leg 1	Leg 2	Leg 3
Length of the upper leg	100mm	100mm	100mm
Length of the lower leg	80mm	80mm	80mm
L. of outmost flexure	60mm	60mm	60mm
L. of inmost flexure	60mm	60mm	60mm
Total width of flexures	20mm	40mm	80mm
Thickness of elbow flexures	0.4mm	0.4mm	0.4mm
Dist. of flex. on median piece	2mm	2mm	2mm
Fabr. angle of upper leg	290°	290°	290°
Fabr. angle of outmost flex	100°	100°	100°
k_1	0.90Nm/rad	2.28Nm/rad	2.28Nm/rad
Thickness of hip flexure	0.3mm	0.4mm	0.4mm
Length of hip flexure	20mm	20mm	20mm
Width of hip flexure	20mm	20mm	20mm
Slider's stopper's offset	-	10mm	15mm
Length of slider flexures	-	50mm	80mm
Width of slider flexures	-	30mm	30mm
Thickness of slider flexures	-	0.15mm	0.3mm

TABLE XII: Tuned PRBM parameters

I. Ansys FEM

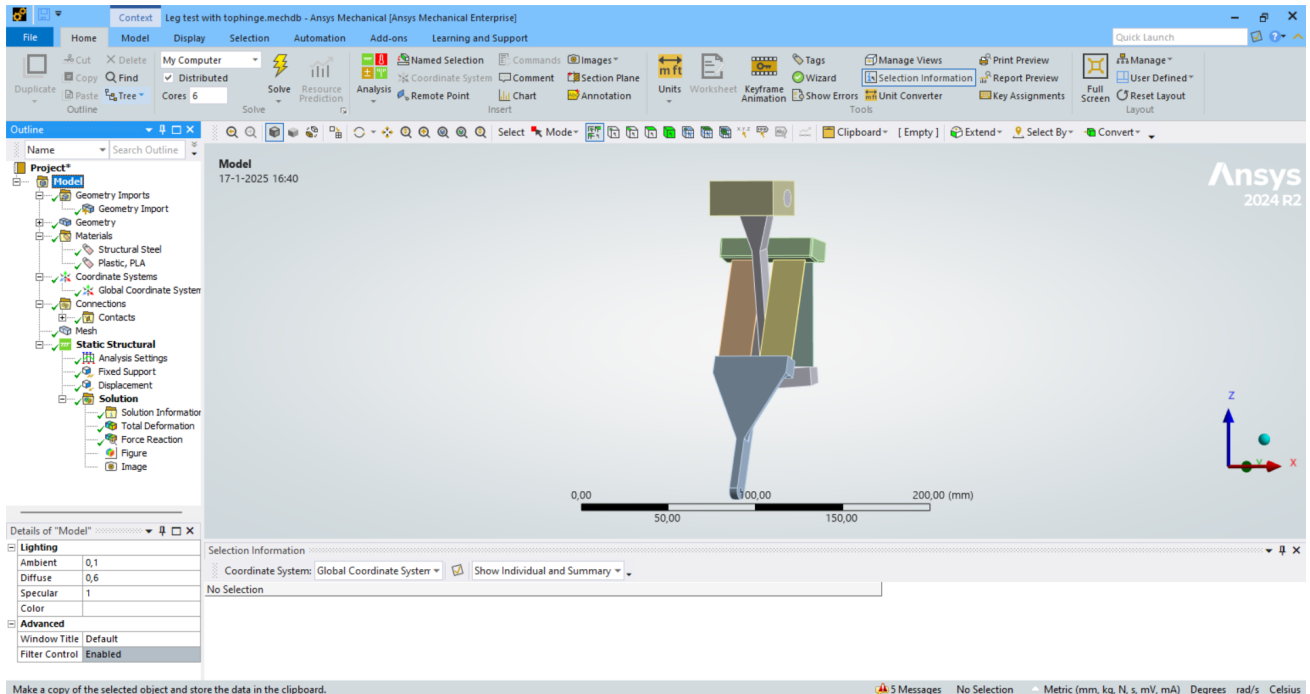


Fig. 32: Full Ansys screen

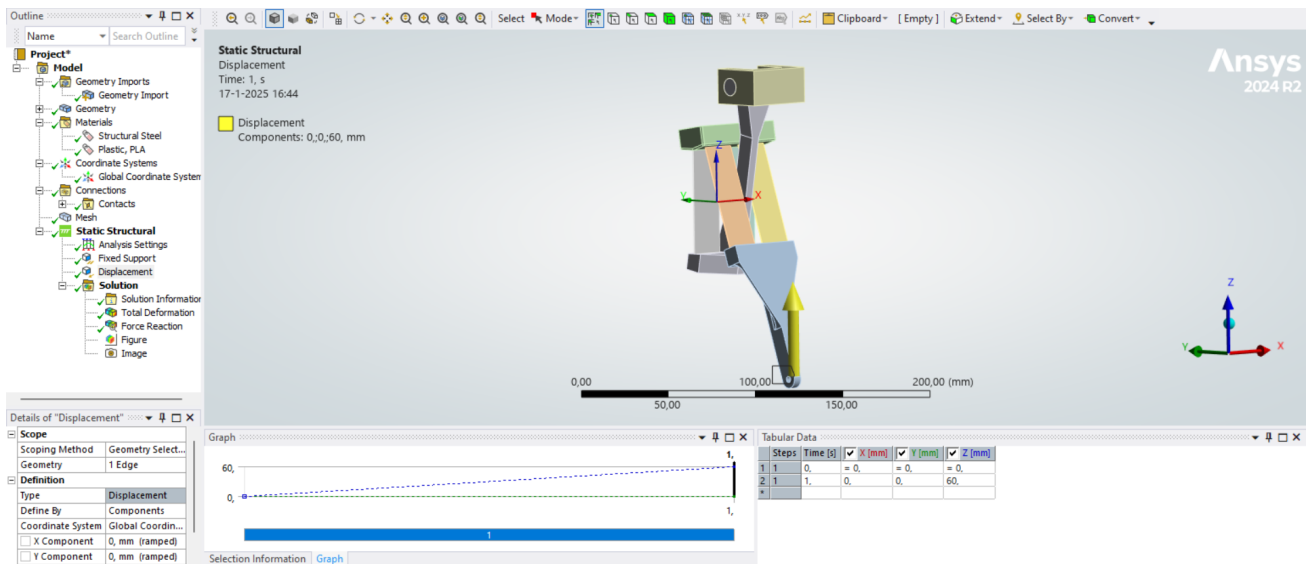


Fig. 33: Ansys displacement total

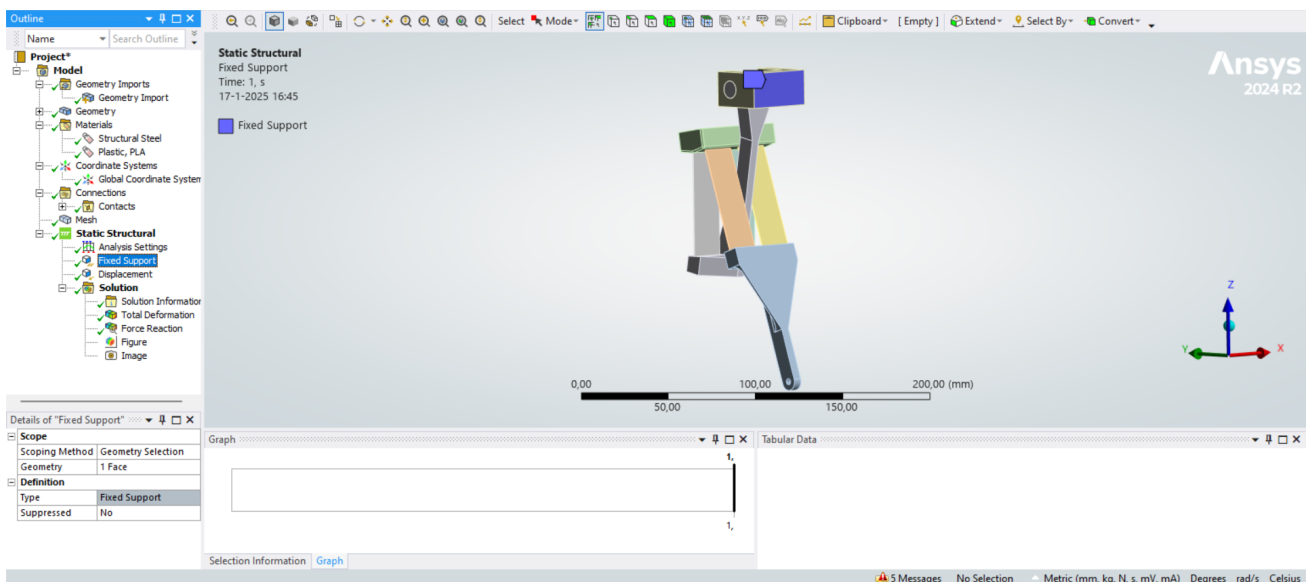


Fig. 34: Ansys fixed support total

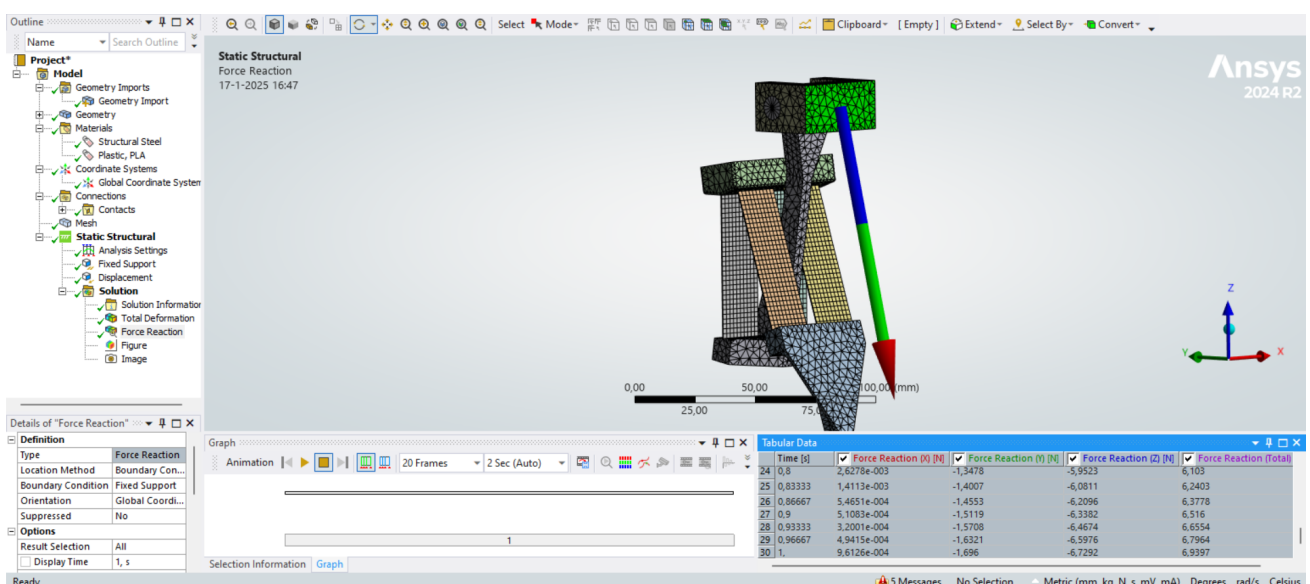


Fig. 35: Ansys force reaction result

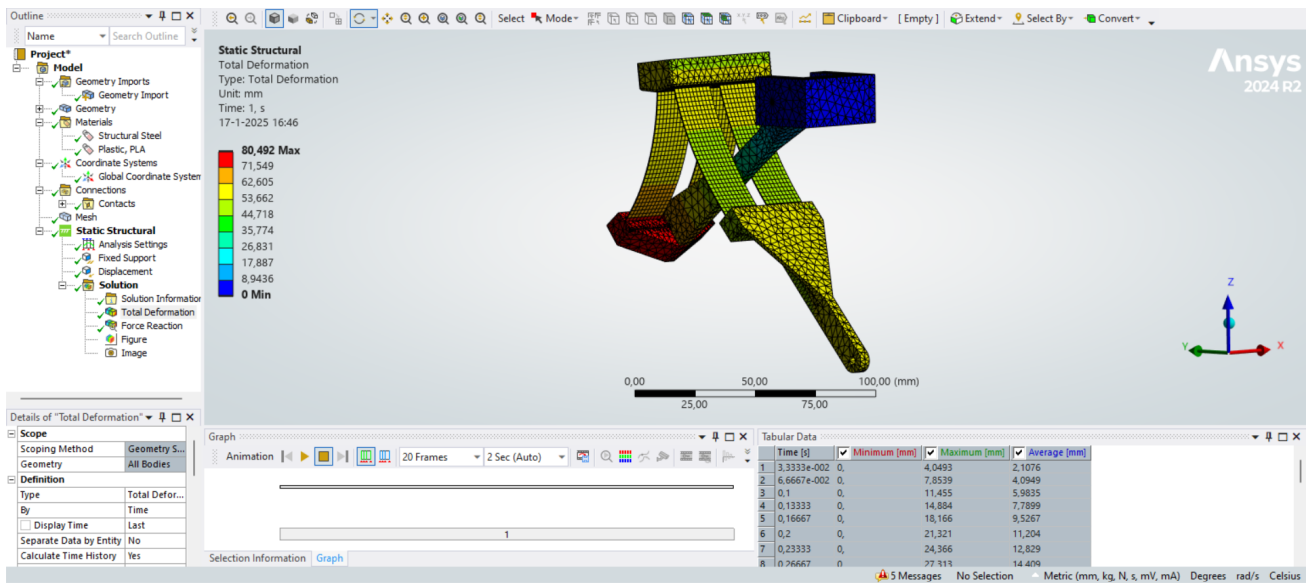


Fig. 36: Final operation angle mechanism

2x20 width	x	y	z	total	2x40 width	x	y	z	total	2x10 width	x	y	z	total
3,33E-02	1,23E-03	-0,11518	-0,70691	0,71623	3,33E-02	3,94E-04	-0,23384	-1,4351	1,454	3,33E-02	3,23E-04	-5,71E-02	-0,34974	0,35437
6,67E-02	2,66E-03	-0,21038	-1,2755	1,2927	6,67E-02	1,43E-03	-0,4283	-2,5963	2,6314	6,67E-02	2,75E-04	-0,10401	-0,62996	0,63849
0,1	4,19E-03	-0,29199	-1,7483	1,7725	0,1	2,72E-03	-0,5956	-3,5661	3,6155	0,1	1,06E-03	-0,14401	-0,86187	0,87382
0,13333	3,54E-03	-0,36391	-2,1518	2,1824	0,13333	2,69E-03	-0,74305	-4,39305	4,4559	0,13333	1,67E-03	-0,17908	-1,0587	1,0737
0,16667	2,41E-03	-0,42881	-2,5035	2,5399	0,16667	2,39E-03	-0,87558	-5,1117	5,1862	0,16667	1,88E-03	-0,21047	-1,2291	1,247
0,2	2,91E-03	-0,48842	-2,8149	2,857	0,2	1,05E-03	-0,99673	-5,7446	5,8305	0,2	1,63E-03	-0,23915	-1,3791	1,3997
0,23333	2,20E-03	-0,54399	-3,0946	3,142	0,23333	8,45E-04	-1,1092	-6,3099	6,4066	0,23333	1,56E-03	-0,26586	-1,5133	1,5365
0,26667	1,47E-03	-0,59649	-3,3487	3,4014	0,26667	2,98E-04	-1,215	-6,8205	6,9279	0,26667	1,68E-03	-0,29104	-1,6348	1,6605
0,3	1,79E-03	-0,64672	-3,5819	3,6398	0,3	9,60E-05	-1,3156	-7,2867	7,4045	0,3	1,05E-03	-0,31507	-1,746	1,7742
0,33333	3,10E-03	-0,69509	-3,7977	3,8607	0,33333	1,39E-03	-1,4122	-7,7161	7,8442	0,33333	4,41E-04	-0,33827	-1,8486	1,8793
0,36667	3,15E-03	-0,74217	-3,9989	4,0672	0,36667	1,68E-03	-1,5059	-8,1115	8,2535	0,36667	8,33E-04	-0,36075	-1,9441	1,9773
0,4	2,20E-03	-0,78818	-4,1877	4,2613	0,4	1,98E-03	-1,5973	-8,4881	8,6371	0,4	1,09E-03	-0,38276	-2,0337	2,0694
0,43333	1,55E-03	-0,83346	-4,366	4,4448	0,43333	1,79E-03	-1,6872	-8,8396	8,9991	0,43333	-1,54E-03	-0,40441	-2,1182	2,1565
0,46667	1,59E-03	-0,87827	-4,5353	4,6195	0,46667	1,32E-03	-1,7761	-9,1726	9,343	0,46667	-1,73E-03	-0,42581	-2,1985	2,2393
0,5	1,35E-03	-0,92288	-4,6969	4,7867	0,5	5,49E-04	-1,8646	-9,4901	9,6715	0,5	-1,29E-03	-0,44708	-2,275	2,3185
0,53333	2,26E-03	-0,96753	-4,852	4,9475	0,53333	2,13E-04	-1,953	-9,7943	9,9871	0,53333	-1,08E-03	-0,46834	-2,3485	2,3948
0,56667	3,50E-03	-5,0015	5,103	0,56667	8,57E-04	-2,0419	-10,087	10,292	0,56667	-7,62E-04	-0,48973	-2,4195	2,4685	
0,6	3,86E-03	-1,0578	-5,1464	5,254	0,6	9,43E-04	-2,1315	-10,371	10,587	0,6	-6,56E-04	-0,51139	-2,4883	2,5403
0,63333	4,13E-03	-1,1037	-5,2872	5,4012	0,63333	1,38E-03	-2,2223	-10,646	10,875	0,63333	-2,37E-04	-0,53341	-2,5554	2,6105
0,66667	3,72E-03	-1,1503	-5,4247	5,5453	0,66667	1,78E-03	-2,3145	-10,915	11,157	0,66667	2,65E-04	-0,55583	-2,6211	2,6794
0,7	3,65E-03	-1,1979	-5,5594	5,687	0,7	2,10E-03	-2,4085	-11,178	11,434	0,7	-9,78E-04	-0,57869	-2,6855	2,7472
0,73333	3,71E-03	-1,2466	-5,6919	5,8268	0,73333	1,68E-03	-2,5046	-11,436	11,708	0,73333	-1,61E-03	-0,60209	-2,749	2,8142
0,76667	2,67E-03	-1,2965	-5,8227	5,9653	0,76667	1,92E-03	-2,6032	-11,692	11,978	0,76667	-1,12E-03	-0,62609	-2,8118	2,8807
0,8	2,63E-03	-1,3478	-5,9523	6,103	0,8	1,92E-03	-2,7046	-11,945	12,247	0,8	-4,47E-04	-0,65078	-2,8742	2,9469
0,83333	1,41E-03	-1,4007	-6,0811	6,2403	0,83333	1,49E-03	-2,809	-12,196	12,515	0,83333	5,56E-04	-0,67627	-2,9363	3,0131
0,86667	5,47E-04	-1,4553	-6,2096	6,3778	0,86667	1,46E-03	-2,917	-12,447	12,784	0,86667	5,10E-04	-0,70269	-2,9984	3,0796
0,9	5,11E-04	-1,5119	-6,3382	6,516	0,9	1,45E-03	-3,0289	-12,698	13,054	0,9	-5,76E-05	-0,73014	-3,0607	3,1466
0,93333	3,20E-04	-1,5708	-6,4674	6,6554	0,93333	1,24E-03	-3,1452	-12,949	13,326	0,93333	-9,26E-04	-0,75868	-3,1235	3,2143
0,96667	4,94E-04	-1,6321	-6,5976	6,7964	0,96667	2,12E-03	-3,2661	-13,203	13,601	0,96667	-1,53E-03	-0,78844	-3,1868	3,2829
1	9,61E-04	-1,696	-6,7292	6,9397	1	2,04E-03	-3,3924	-13,46	13,881	1	-1,96E-03	-0,81955	-3,251	3,3527

Fig. 37: Results from Ansys in 30 steps, every step is 2mm; x, y, z, total are in Newtons

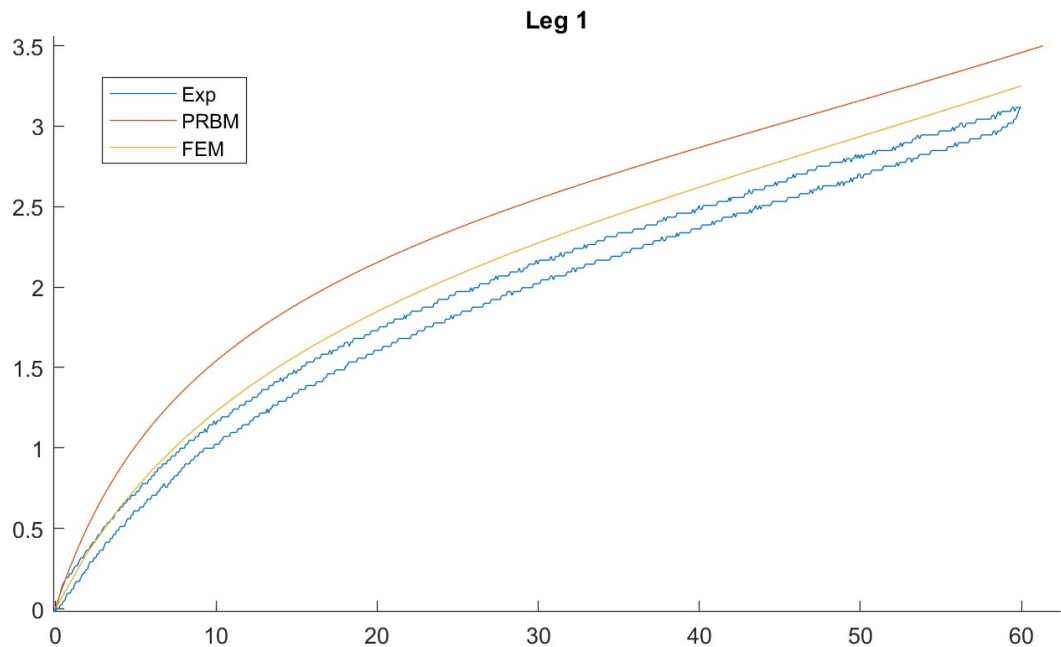
J. First Test Elbow Stiffness Results

Fig. 38: F/D curves comparison, leg 1 test 1

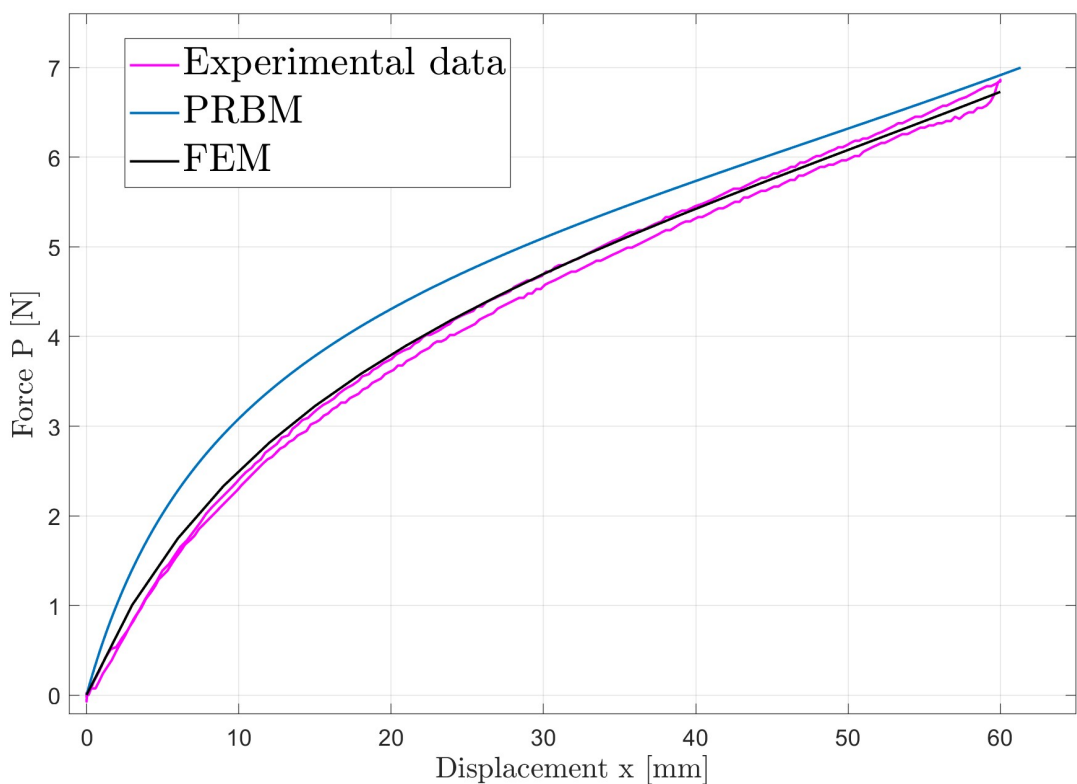


Fig. 39: F/D curves comparison, leg 2 test 1

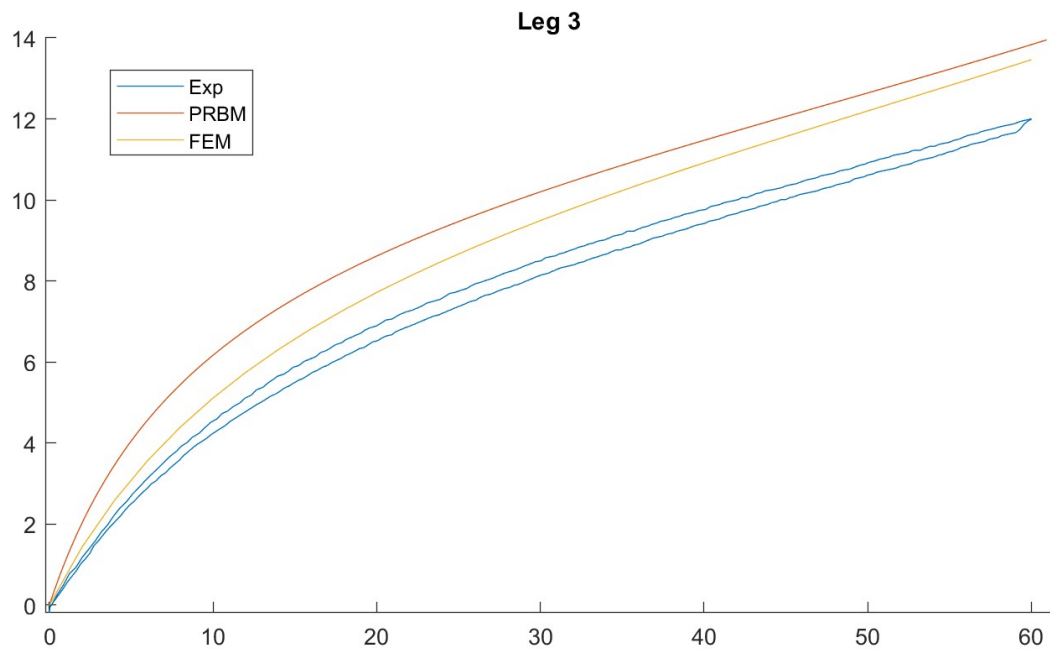


Fig. 40: F/D curves comparison, leg 3 test 1

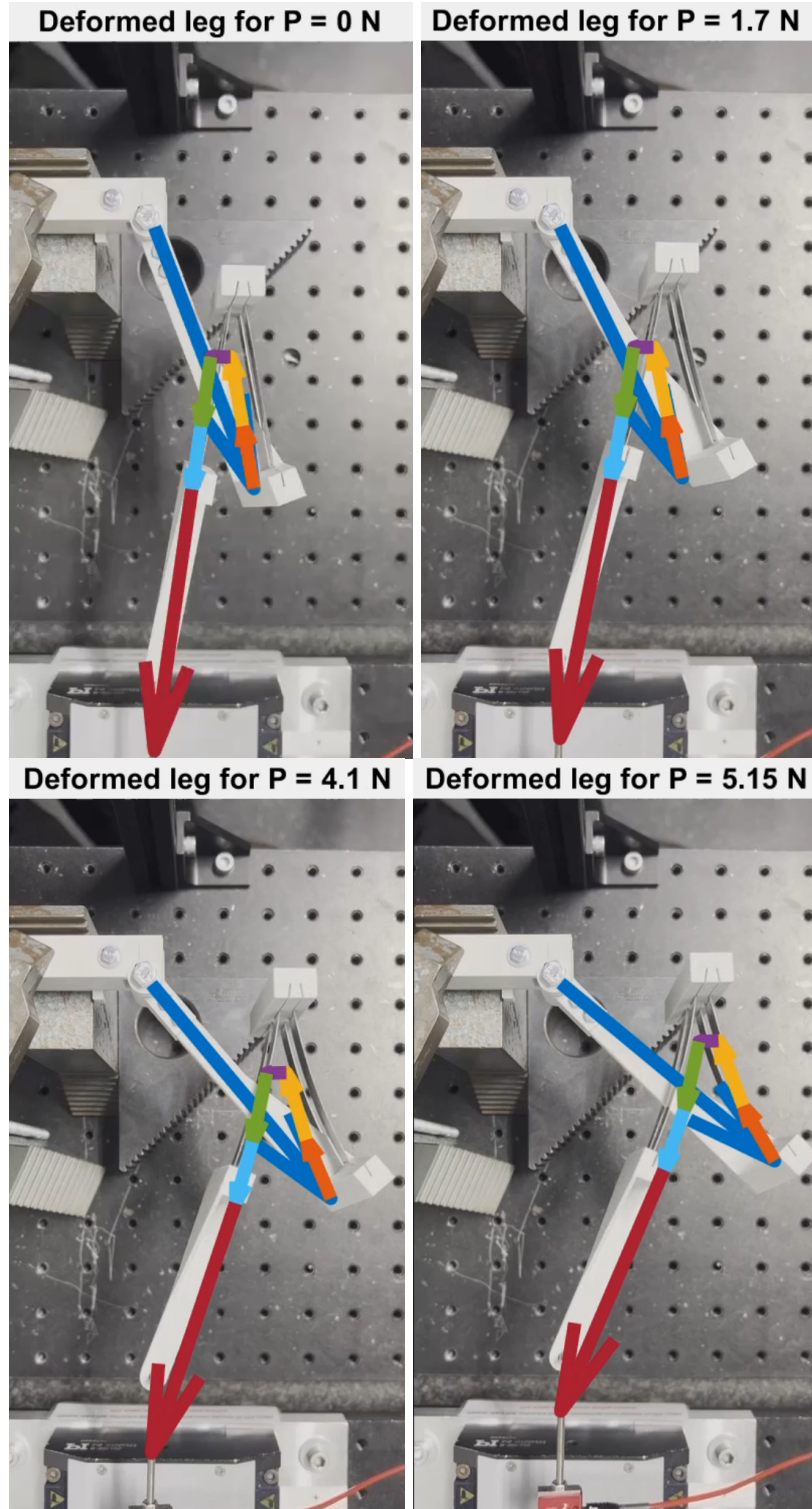
K. First Test Video Overlay

Fig. 41: Leg Tets PRBM Video Overlay

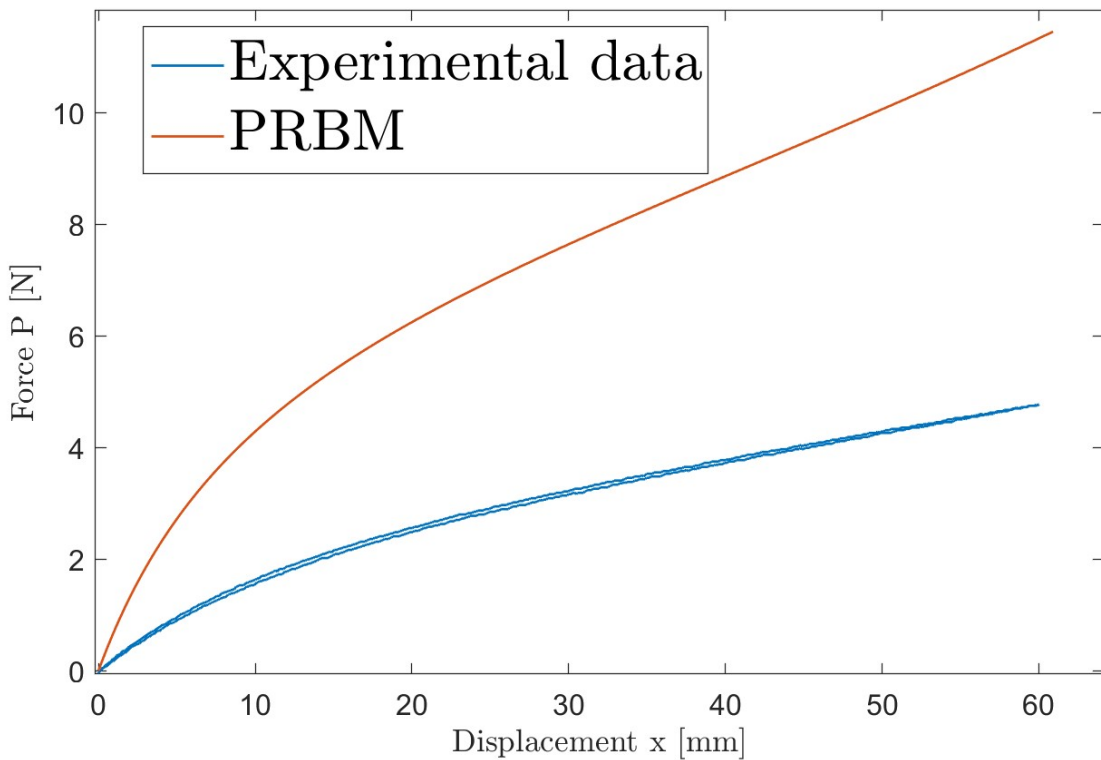
L. Second Test Results

Fig. 42: F/D curve comparison, leg 1, test 2

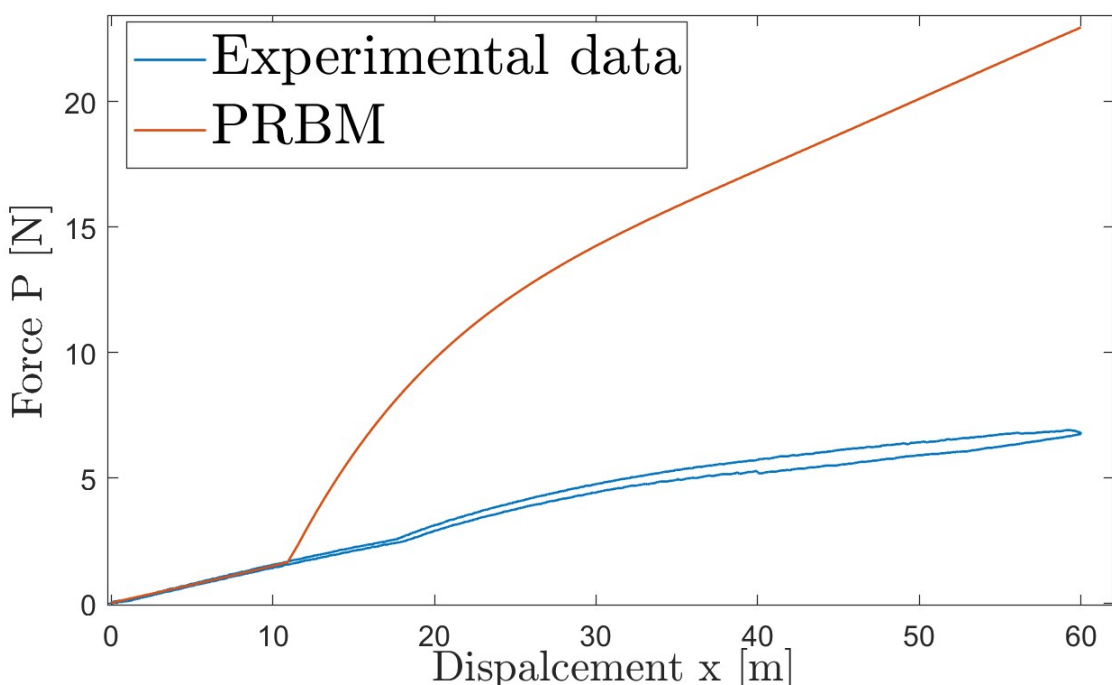


Fig. 43: F/D curve comparison, leg 2, test 2

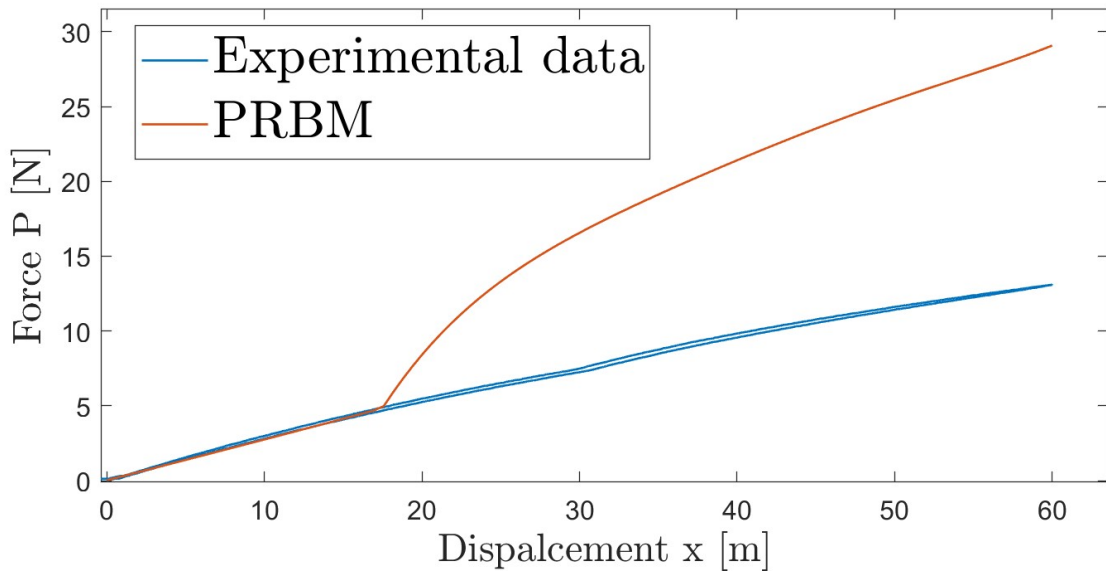


Fig. 44: F/D curve comparison, leg 3, test 2

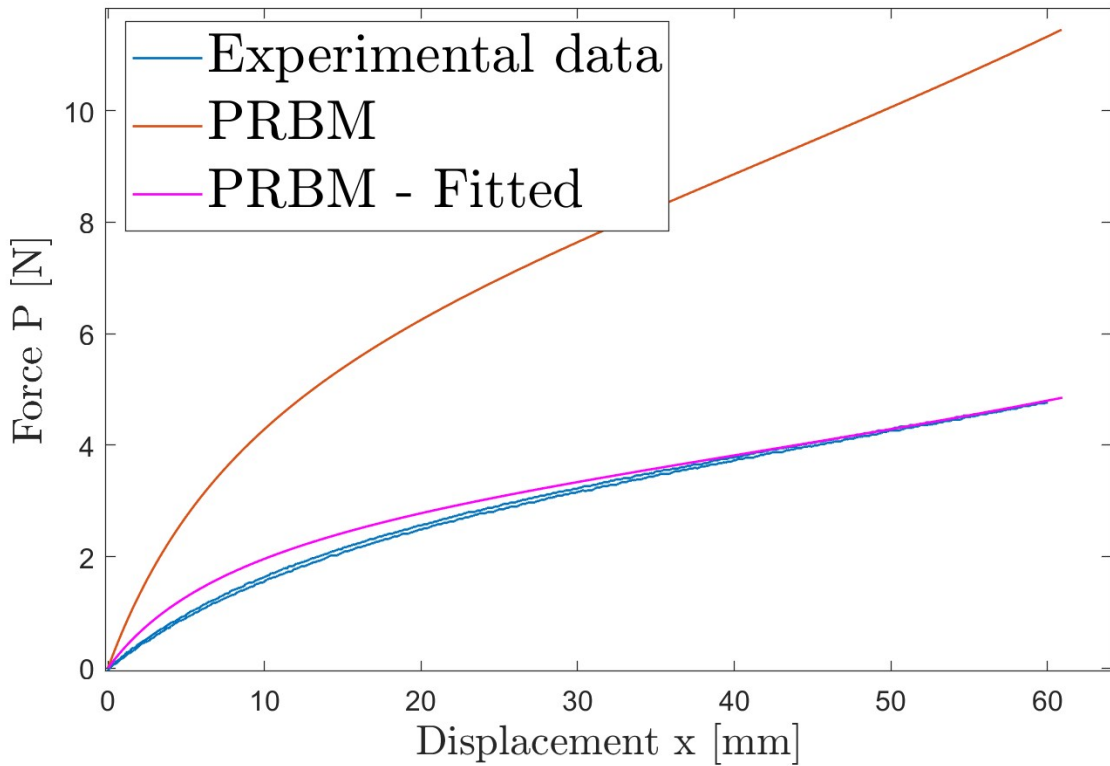
M. Second Test PRBM retuning

Fig. 45: F/D curve fitting, leg 1, test 2

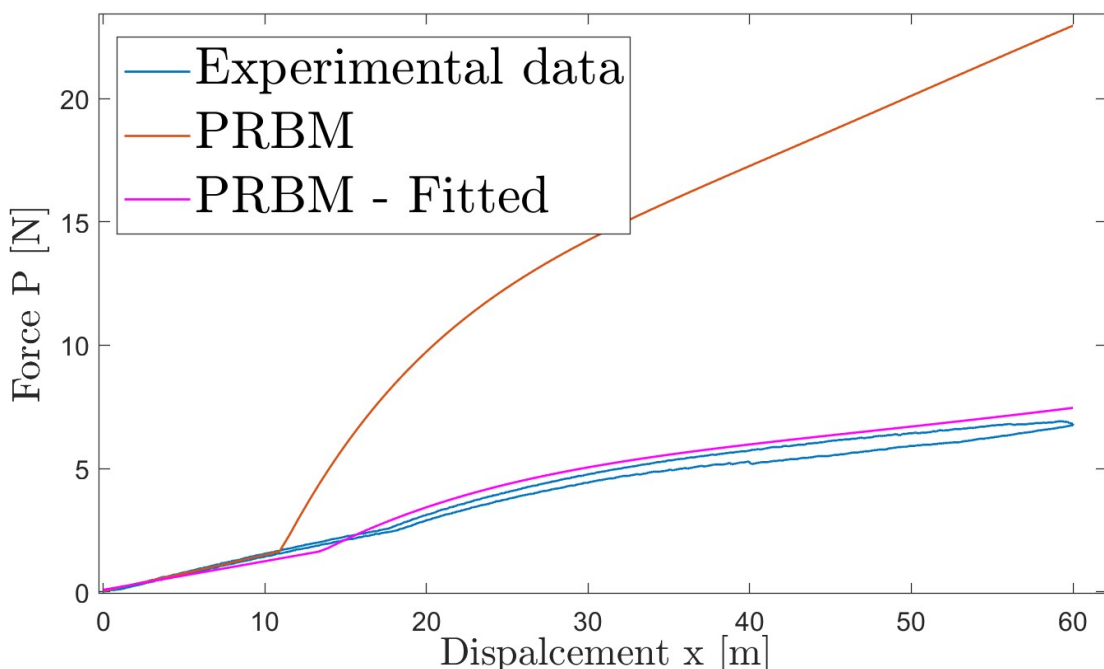


Fig. 46: F/D curve fitting, leg 2, test 2

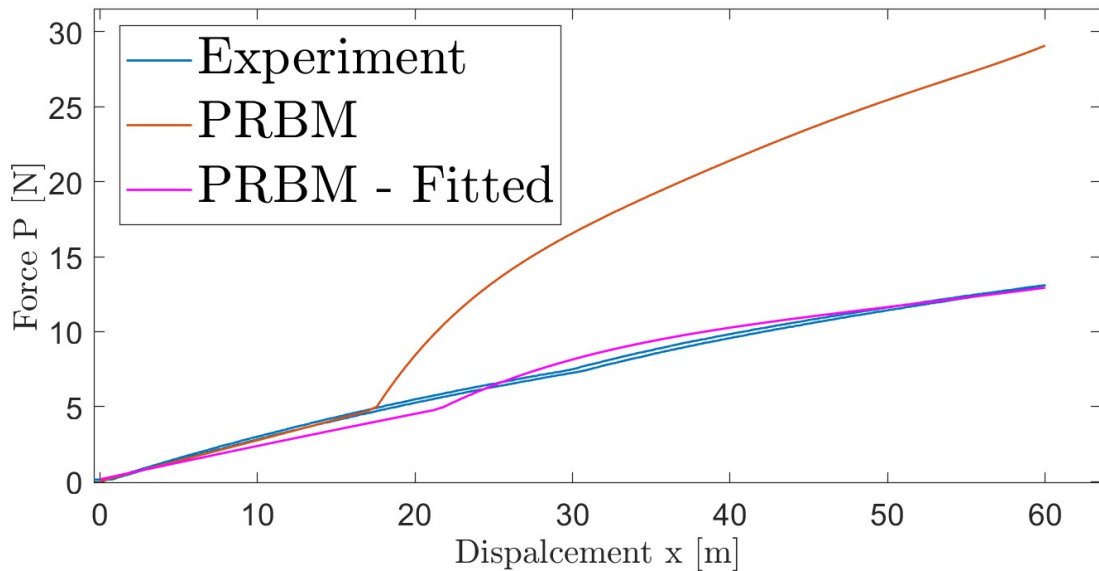


Fig. 47: F/D curve fitting, leg 3, test 2

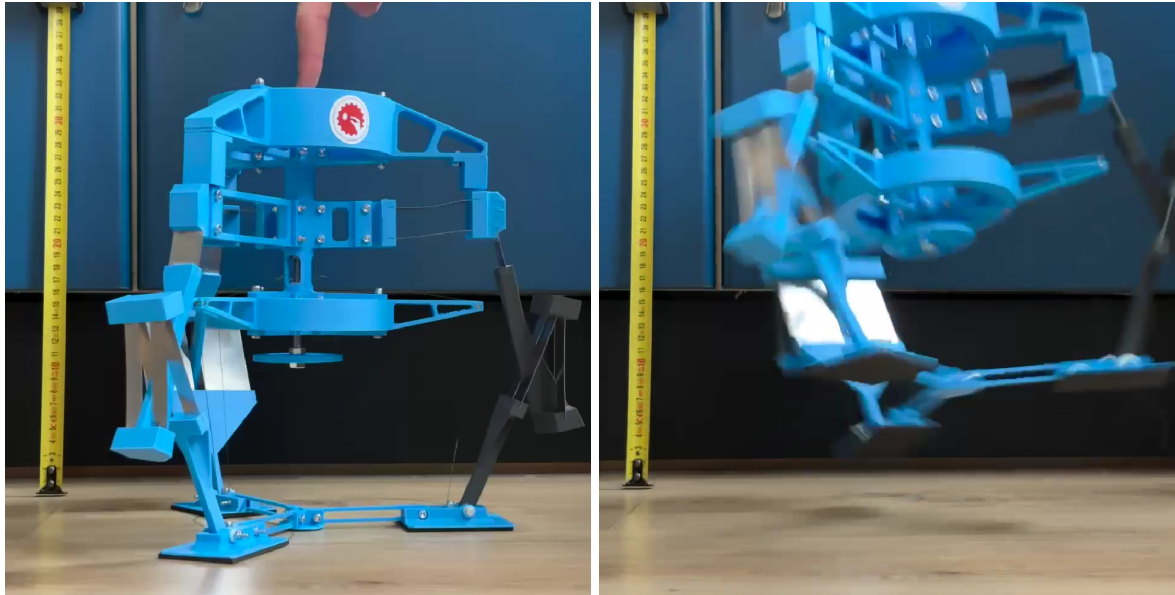
N. Jump Test

Fig. 48: Vertical Jump



Fig. 49: Horizontal Jump

O. Symposium Presentation Slides

Symposium Pitch

ME46055-23 Compliant Mechanics

13/01/2025

Sil Barendregt

Roman Bosch

Fabio Milazzo

Martijn Schrama

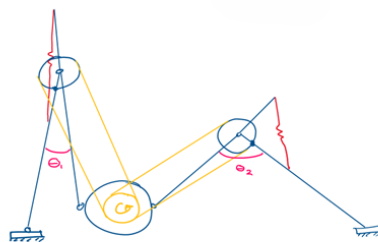


Fig. 50: Slide 1

Design Case

Product usecase

What?

To design a Lunar Probe that traverses the terrain by jumping in different directions

How?

A path/motion generator utilizing classic linkage systems turned compliant

Why Compliance?

To combine the mechanical energy source with linkage mechanics.
Reduces mass and increased reliability



<https://www.nasa.gov/history/alsj/>

2

Fig. 51: Slide 2

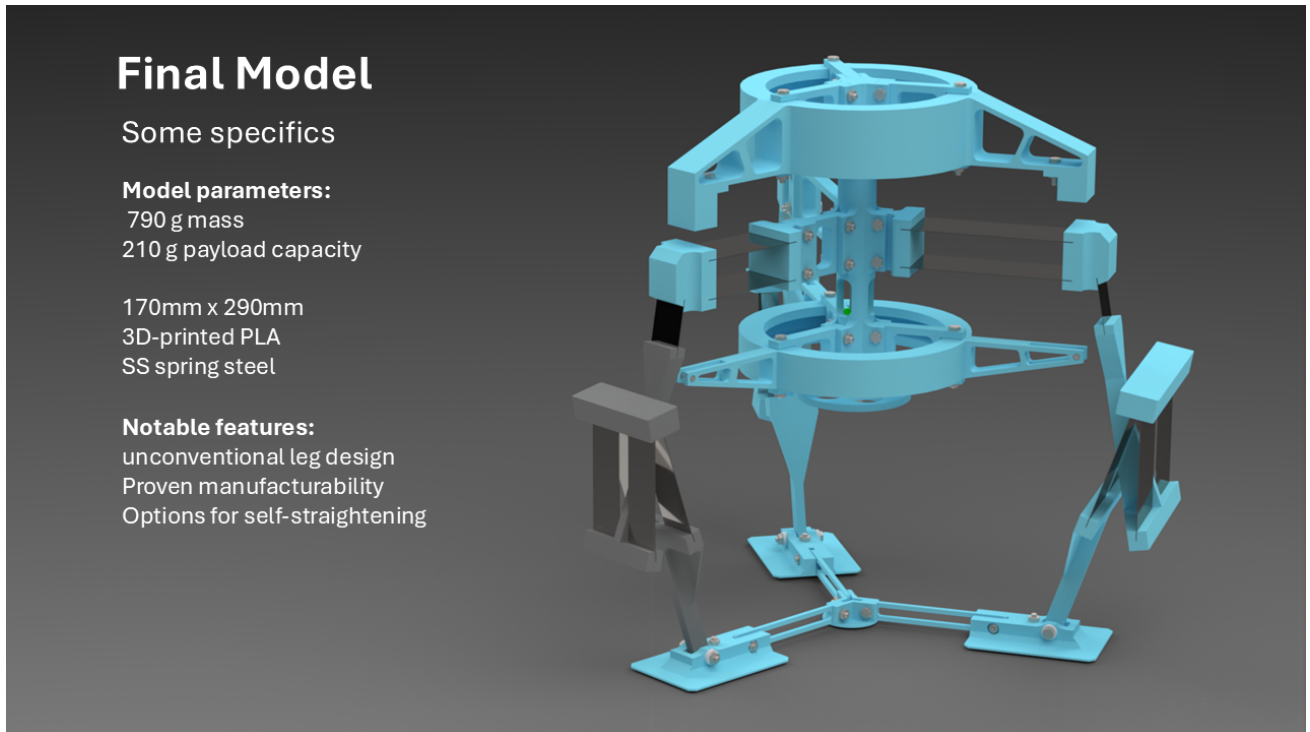


Fig. 52: Slide 3

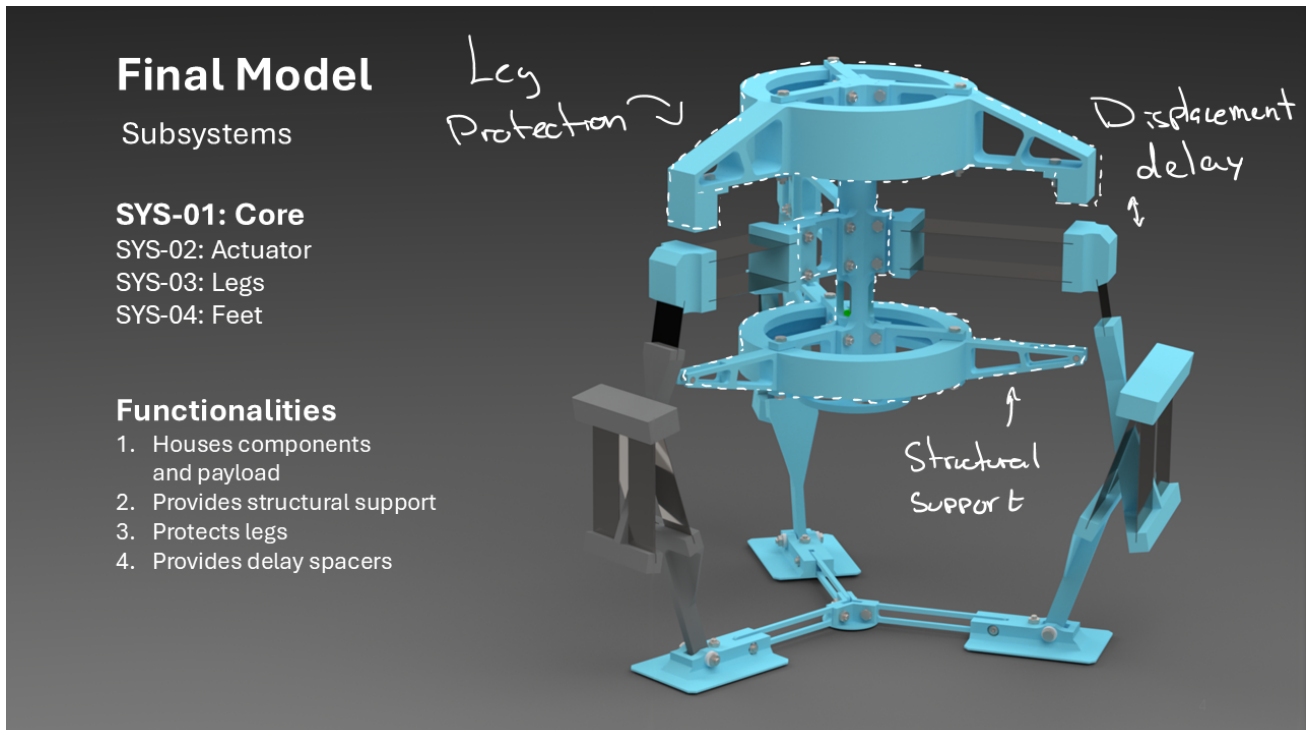


Fig. 53: Slide 4

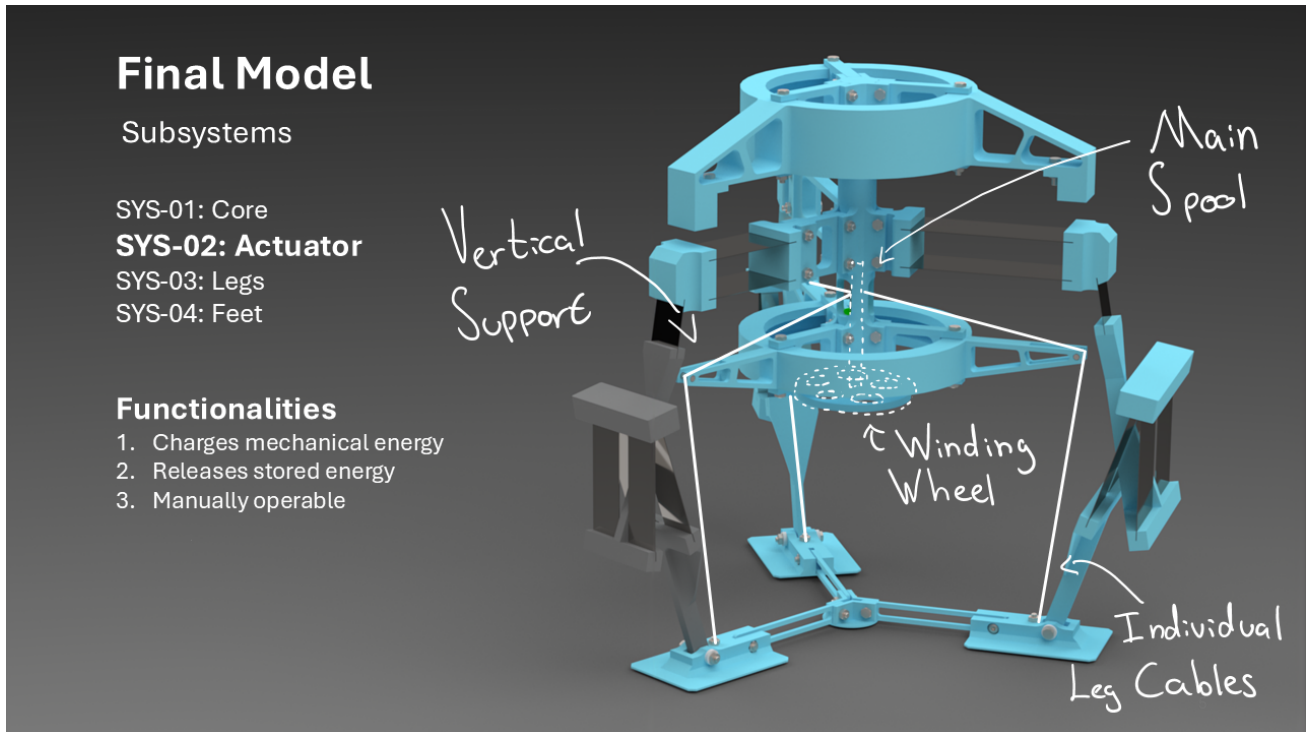


Fig. 54: Slide 5

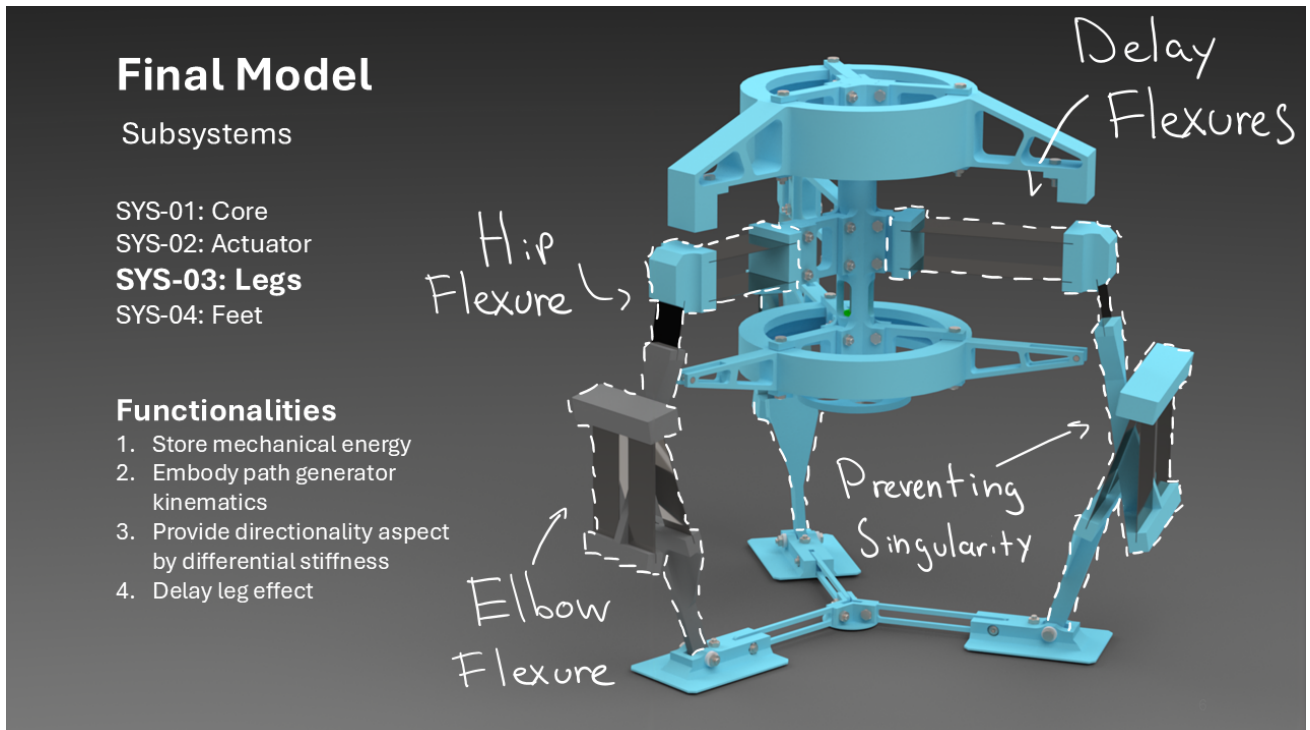


Fig. 55: Slide 6

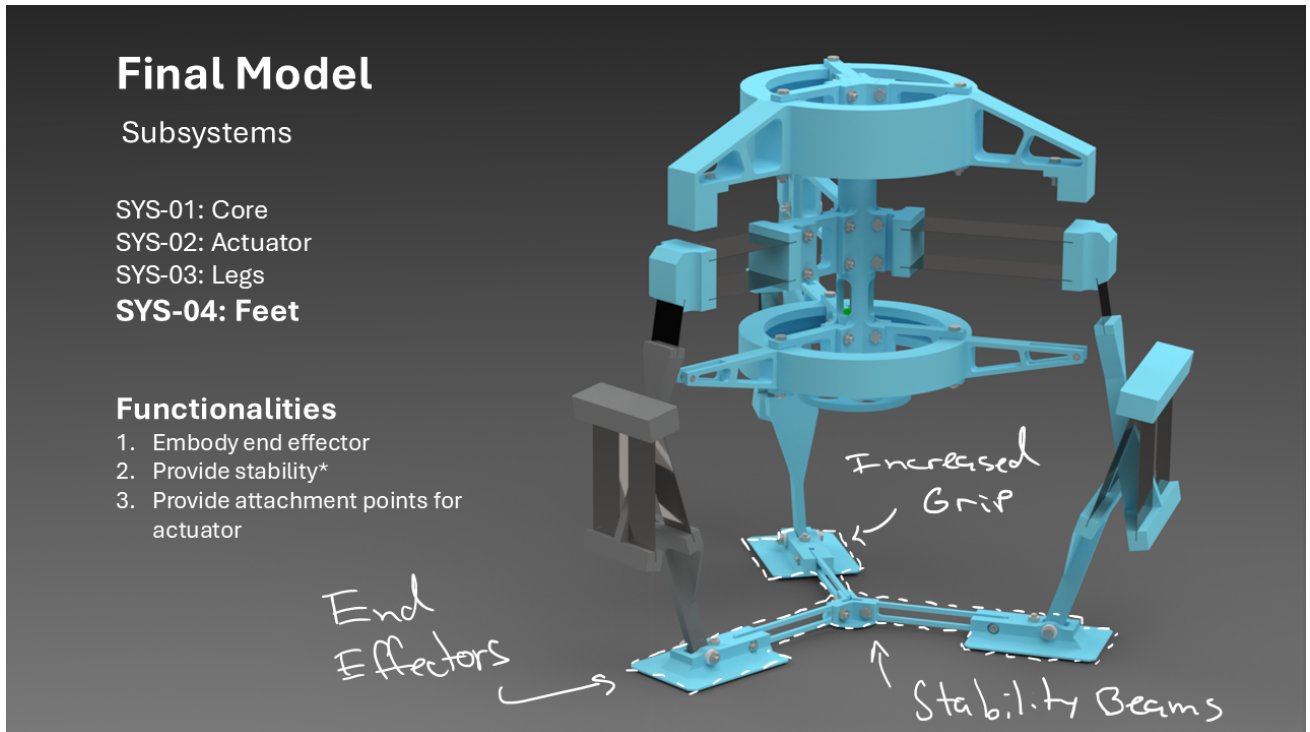


Fig. 56: Slide 7

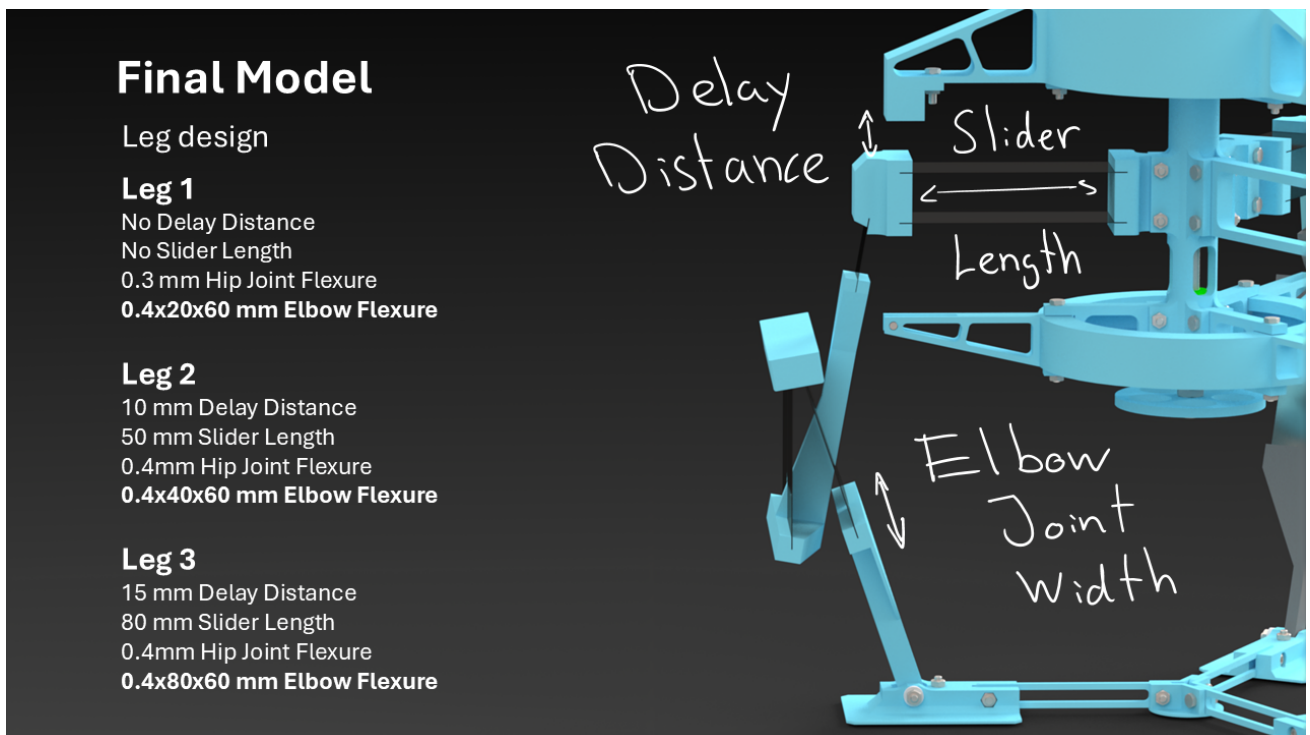


Fig. 57: Slide 8

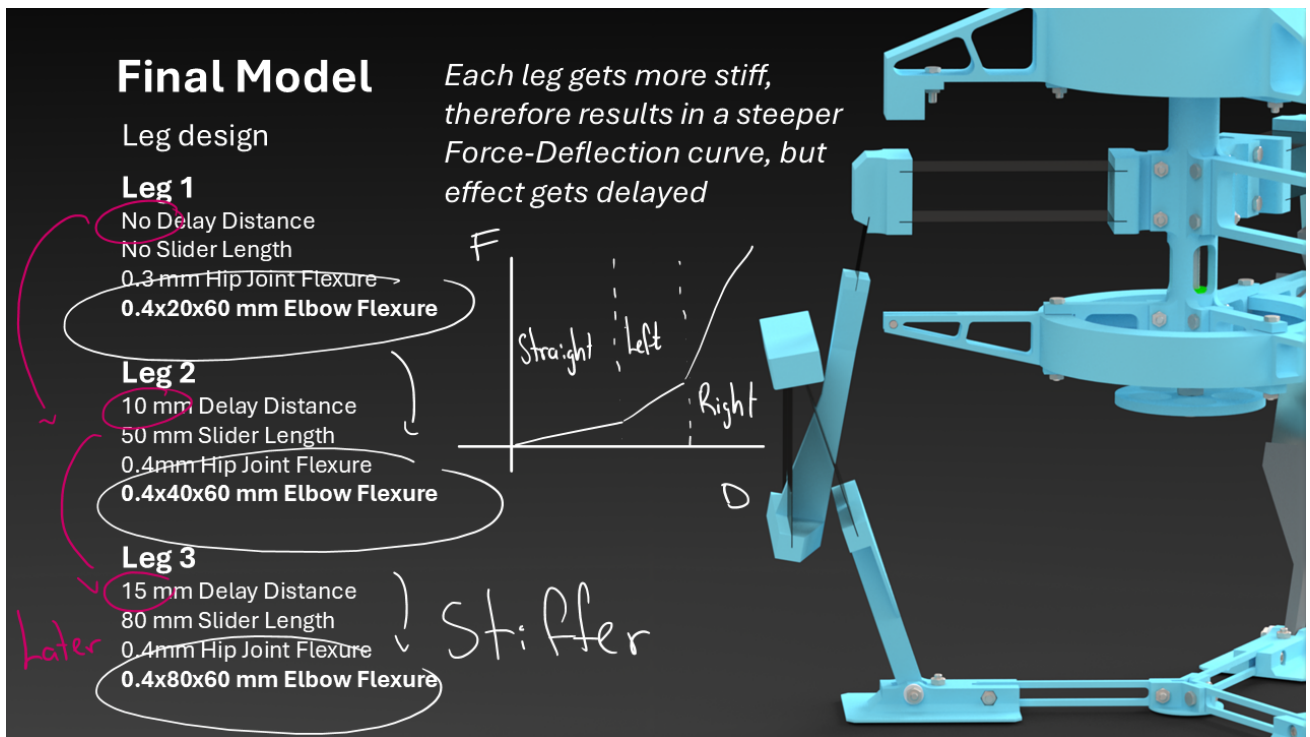


Fig. 58: Slide 9

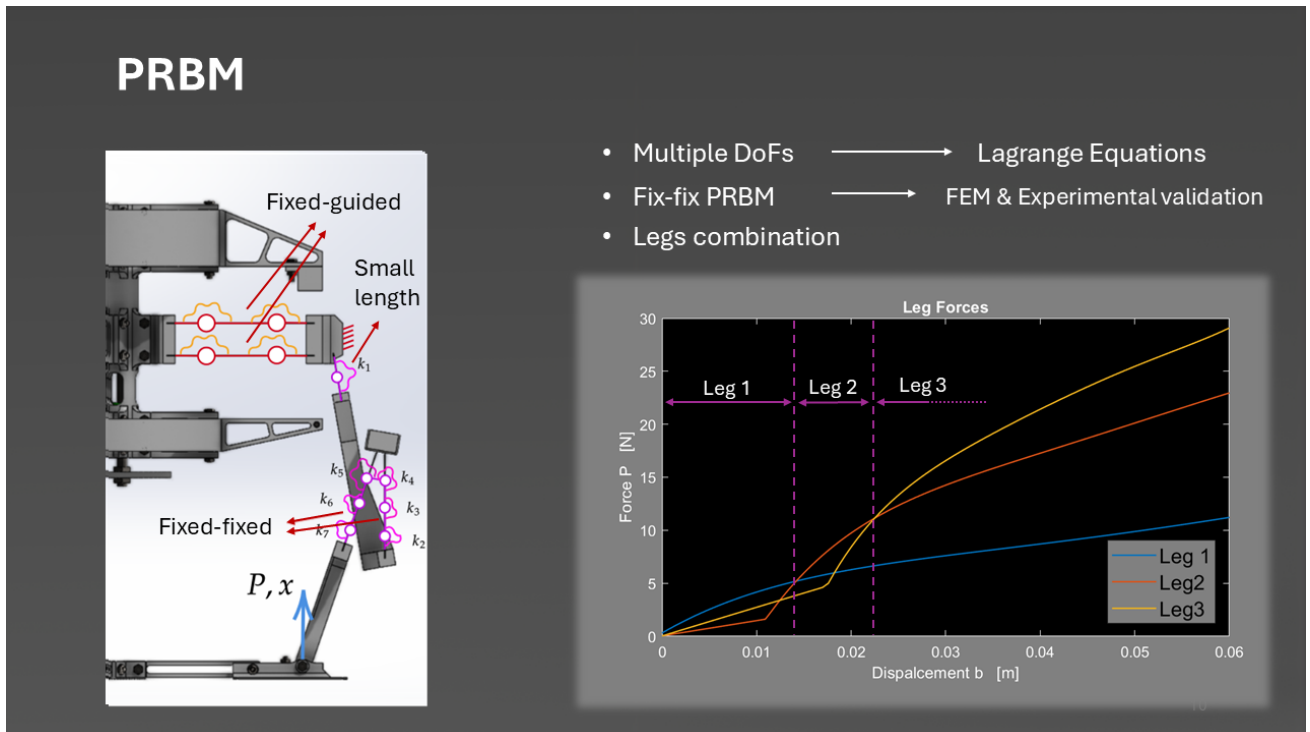


Fig. 59: Slide 10

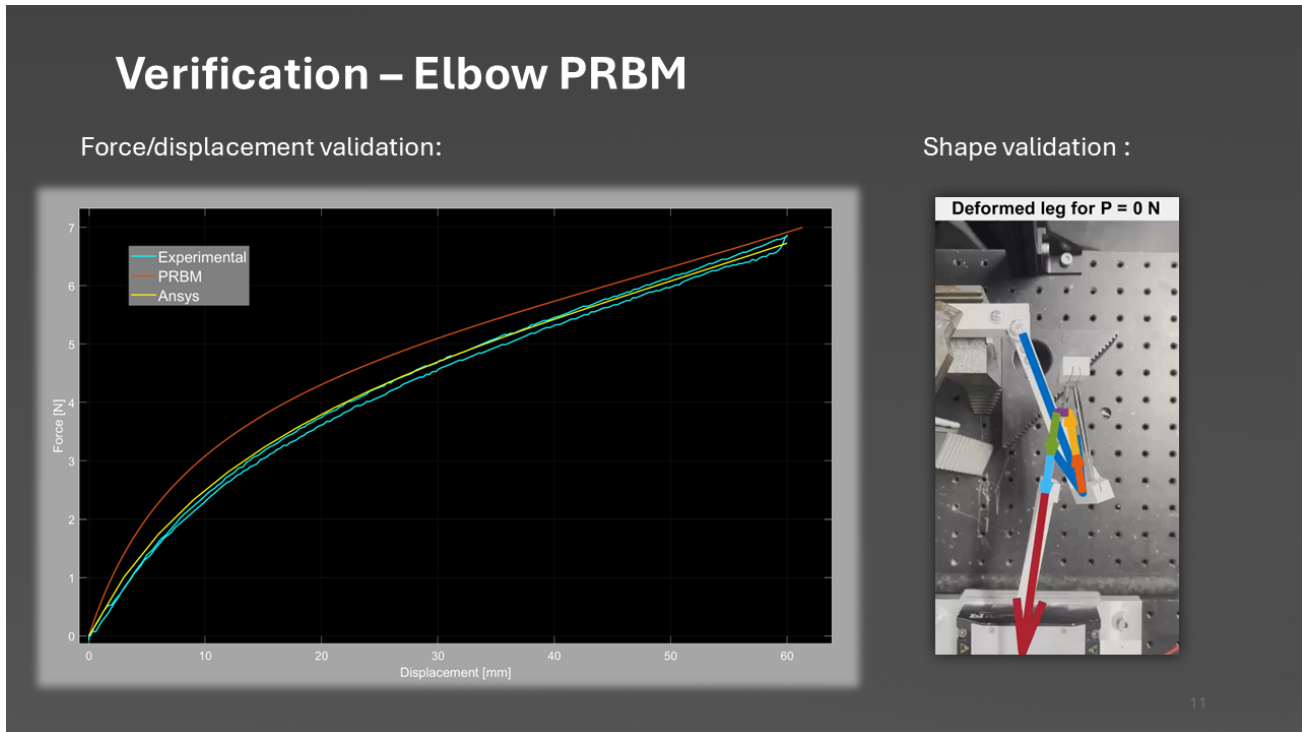


Fig. 60: Slide 11

Discussion and Future work

Product Evaluation

Functionality achieved?

Jumping height **too small**

All other requirements **achieved!**

Reusability

Compliance to store energy

Release energy

Payload capabilities

Payload and component protection

...

Any model improvements?

Weight can be **reduced**

Improved materials for better mass/strength ratio

Redesign actuator for autonomous use



12

Fig. 61: Slide 12

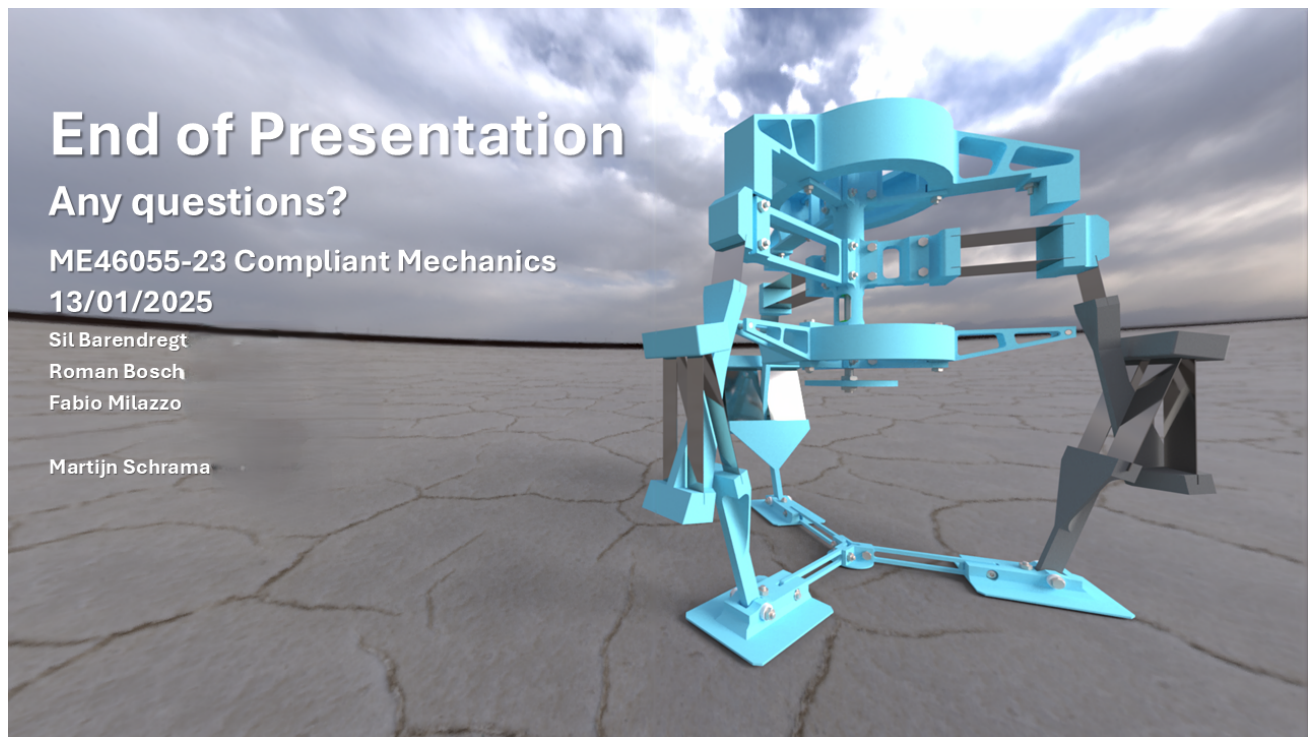


Fig. 62: Slide 13

Appendix Slides

Fig. 63: Slide 14

Functional Analysis

Product Functions Functional Requirements Design Conditions Performance Criteria

"What does the product have to do?"

ID	Functions	Unit/ additional info
PROD-01	The Jumper traverses a horizontal and vertical distance	1 kg
PROD-02	The Jumper can take a measurement at the apogee of the jump	Photo, atmospheric measurement, acceleration: modular payload
PROD-03	The Jumper continues to jump in a desired direction after it has been set off	The Jumper is a pseudo autonomous system

15

Fig. 64: Slide 15

Functional Analysis

Product Functions Functional Requirements Design Conditions Performance Criteria

"How will the product achieve its functionality?"

ID	Requirement	Unit/ additional info
FUNC-01	The Jumper is reusable	100 cycles
FUNC-02	The Jumper straightens itself	
FUNC-03	The Jumper can be "charged" by either itself or an operator	
FUNC-04	The Jumper stores mechanical energy	Joule
FUNC-05	The Jumper releases the stored energy to jump	
FUNC-06	The Jumper can jump in a desired direction	Angle
FUNC-07	The Jumper jumps 5 meters up in the air	Meters
FUNC-08	The Jumper can span a distance of 5 meters horizontally	Meters
FUNC-09	The Jumper detects the apogee	
FUNC-10	The Jumper takes the photo/ measurement	
FUNC-11	The Jumper stores the photo/measurement	
FUNC-12	The Jumper falls down to earth	
FUNC-13	The Jumper protects its equipment from impact	Impact force (N)

16

Fig. 65: Slide 16

Functional Analysis

Product Functions Functional Requirements **Design Conditions** Performance Criteria

"What are the conditions that limit the design freedom?"

ID	Condition	Unit/ additional info
COND-01	The Jumper has a maximum mass	1 kg
COND-02	The Jumper stores energy by means of compliant mechanics	n.a.
COND-03	The materials used should be able to endure space conditions	Temperature, Radiation, Vacuum properties

17

Fig. 66: Slide 17

PRBM

Selection procedure

	Parallel \\ Stifness	Series s
	$k_{\parallel} = \left(\sum \frac{1}{k_i} \right)^{-1}$	$k_s = \sum k_i$
Displacement	$x = x_i$	$x = \sum x_i$

Ideally:

- High angular displacement – to allow for longer range of motion
- High off axis stiffness – since a lot of force will be transmitted
- Low stiffness – it can be increased through a series configuration

18

Fig. 67: Slide 18

Design process

- What's next?

- Rough PRBM and FEM

- To obtain some starter values for the elbow flexures
 - In combination with linear beam theory



- Pure Elbow Tests

- To obtain effective stiffnesses of the elbow joints



- Complete PRBM

- Include found K_eff in complete system PRBM
 - Additional tuning options



- Complete System Test

- Verify FEM and Complete PRBM

In the industry, PRBMs often only provide preliminary values to narrow down ranges for initial guesses of dimensions.

Computational methods like FEM provide more concise system behaviour expectations.

Fig. 68: Slide 19